Journal of Petrology Advance Access published July 6, 2010

Re-evaluation of Rapakivi Petrogenesis: Source Constraints from the Hf Isotope Composition of Zircon in the Rapakivi Granites and Associated Mafic Rocks of Southern Finland

A. P. HEINONEN[1]*, T. ANDERSEN[2] AND O. T. RÄMÖ[1]

[1]DEPARTMENT OF GEOLOGY, PO BOX 64, FIN-00014, UNIVERSITY OF HELSINKI, HELSINKI, FINLAND
[2]DEPARTMENT OF GEOSCIENCES, UNIVERSITY OF OSLO, PO BOX 1047, BLINDERN, N-0316 OSLO, NORWAY

RECEIVED DECEMBER 10, 2009; ACCEPTED JUNE 8, 2010

The 1650–1540 Ma rapakivi granites and associated basic rocks (e.g. gabbro–anorthosites) in southern Finland intrude the local juvenile Paleoproterozoic crust with little isotopic contrast to the contemporary mantle. Conventional isotopic studies have not been able to provide a satisfactory answer to the long-running controversy over the sources involved in their petrogenesis. In situ *zircon laser ablation inductively coupled plasma mass spectrometry analysis of Lu–Hf isotopes and trace elements has been used to resolve the source and magmatic evolution of the rapakivi granites and associated massif-type anorthositic rocks in southern Finland. Initial Hf isotope compositions of zircon extracted from the rapakivi granites are relatively homogeneous and overlap with the modeled evolution of the Paleoproterozoic crust of southern Finland. Within-sample variation in zircon of the basic rocks is considerably greater than that of the granites and the initial Hf isotope compositions vary from crustal values (ε_{Hf} ~0) to depleted mantle (ε_{Hf} ~+9) values. Furthermore, Ti abundances that correlate with Hf isotope compositions record significant crustal assimilation during crystallization of the mafic magmas. Our* in situ *Hf isotope results enhance the resolution of isotopic methods in pursuit of the sources of the Precambrian rapakivi suites. The new data argue for the truly bimodal nature of rapakivi magmatism, involving at least two distinct magma sources—a relatively homogeneous Paleoproterozoic crustal component for the granites and a depleted, mid-ocean ridge basalt source-like mantle component for the basic rocks.*

KEY WORDS: *Finland; Hf isotopes; rapakivi granites; trace elements; zircon*

INTRODUCTION

A-type granites, as originally defined by Loiselle & Wones (1979), and their volcanic equivalents and related rocks (mafic intrusions, anorthosites, basaltic dikes and lavas, rare alkaline rocks) form a conspicuous part of the granite spectrum. They have been recognized as a specific group only relatively recently (Loiselle & Wones, 1979), and were originally defined as dry (anhydrous) rocks with high contents of alkali metals (either sodium or potassium) and most high field strength trace elements (e.g. Bonin, 2007; Frost *et al.*, 2007). They commonly have been emplaced in an extensional tectonic regime not directly related to lithospheric convergence (i.e. they have been considered 'anorogenic' or 'post-tectonic'). In terms of age, the A-type granites span almost three billion years (~2·7 Ga to Recent) and they are associated with a variety of mineralization types (e.g. Sn, F, Nb, Ta, Au, Fe, U and REE). Chemically the A-type granites can be classified as ferroan calc-alkaline to alkaline–calcic granitoids (Frost *et al.*, 2001).

*Corresponding author. Telephone: +358 9 191 50802.
E-mail: aku.heinonen@helsinki.fi

Proterozoic ferroan rapakivi granites and associated massif-type anorthosites and gabbroic rocks constitute an important part of the traditional A-type clan. Regarding their petrogenesis, a major problem that still awaits solution is the origin of the associated anorthositic and gabbroic rocks and their relation to these granites. Many studies since the 1970s have favored a magmatic underplating model that infers the mantle as the source for the anorthosites and the lower continental crust for the granites (e.g. Emslie, 1978; Anderson, 1983; Haapala & Rämö, 1990; Frost *et al.*, 1999; Scoates & Mitchell, 2000). This view has been challenged more recently by isotopic and experimental studies (e.g. Duchesne & Wilmart, 1997; Vander Auwera *et al.*, 1998; Longhi *et al.*, 1999; Schiellerup *et al.*, 2000) that invoke a lower crustal source for the anorthosite magmas or suggest that the silicic and basic rocks are consanguineous with an intermediate ('jotunitic') precursor.

The crust–mantle source controversy has prevailed in part because of the fact that radiogenic isotope studies utilizing the whole-rock and mineral Sm–Nd, Rb–Sr, Lu–Hf, and Pb–Pb methods have yielded rather similar initial isotope ratios for both the silicic and basic rocks of the association (e.g. Patchett *et al.*, 1981; Rämö, 1991; Neymark *et al.*, 1994; Andersson, 1997). These conventional isotope methods utilize the isotope dilution thermal ionization mass spectrometry (ID-TIMS) technique, which is only able to produce average isotope values for the examined (usually hand-sized) samples. We have used the new *in situ* laser ablation multicollector inductively coupled plasma mass spectrometry (LAM-ICP-MS) technique to measure the Hf isotope composition of single zircon grains separated from selected rapakivi granites, anorthosites, and gabbros in the classic rapakivi granite terrain of southern Finland. Our results imply a clear difference in the initial Hf isotope composition of the rapakivi granites and the basic rocks associated with them, a mantle origin for the anorthosites, and the presence of a major crustal source component in the granites. Surprisingly, our data further reveal a much wider range of initial Hf isotope composition in the zircons from the basic rocks than in those from the silicic rocks. This can be explained by a mantle–crust mixing process that affected the composition of zircon precipitating from the mafic magmas.

GEOLOGICAL SETTING

The Finnish rapakivi granites and associated rocks (e.g. Rämö & Haapala, 2005) comprise four large batholiths (Wiborg, Åland, Laitila and Vehmaa) and a group of smaller plutons (Suomenniemi, Ahvenisto, Onas, Bodom, Obbnäs, Peipohja, Mynämäki, Eurajoki, Reposaari, Siipyy, Fjälskär and Kökarsfjärden) (Fig. 1). The Finnish province is associated with the Salmi rapakivi intrusion in Russian Karelia (Neymark *et al.*, 1994) and the Baltic rapakivi intrusions of Riga, Märjamaa and Naissaare (Rämö *et al.*, 1996). Also, the rapakivi occurrences in central Sweden (e.g. Andersson, 1997) are considered to belong to the same province.

The rapakivi granites of Finland were emplaced between 1650 and 1540 Ma into the 1900–1800 Ma Svecofennian crust and they form two distinct age groups. The 1650–1620 Ma group (southeastern Finland) includes the Wiborg, Suomenniemi, Ahvenisto, Onas, Obbnäs and Bodom batholiths. The 1590–1540 Ma group (southwestern Finland) includes the intrusions of Åland (or Ahvenanmaa), Laitila, Vehmaa, Peipohja, Mynämäki, Reposaari, Siipyy, Eurajoki, Fjälskär and Kökarsfjärd (Rämö & Haapala, 2005).

The Finnish rapakivi granites exhibit typical geochemical features of ferroan alkali–calcic (Frost *et al.*, 2001) granites: high K/Na and Fe/Mg ratios, and enrichment of light rare earth elements (LREE) over heavy REE (HREE) (e.g. Bonin, 2007). In terms of their aluminium saturation, they straddle the boundary between the per- and metaluminous fields. These features are also evident in the reduced nature of their mineralogical composition (fayalite + quartz and magnetite present in the most mafic granitoids) and petrographic features (amphibole and biotite late in the crystallization sequence) resulting from a 'dry' magmatic environment at low oxygen fugacity (Rämö & Haapala, 2005).

The Finnish rapakivi suite is dominantly bimodal (silicic–mafic) with only minor intermediate rock-types. The rapakivi granites generally exhibit a differentiation trend from fayalite and hastingsite granites through biotite-dominated varieties to topaz granites with strong enrichment in incompatible elements including volatiles. The mafic rocks are dominantly anorthositic, mainly leucogabbronorites, and they are considered to belong to the Proterozoic massif-type anorthosite suite (e.g. Ashwal, 1993; Alviola *et al.*, 1999). Rare intermediate compositions are represented by monzodiorites and quartz monzodiorites (e.g. Alviola *et al.*, 1999). The marked compositional gap between the silicic and mafic end-members of the suite is usually taken as evidence of these rock-types not being consanguineous. This conclusion has, however, been challenged in other anorthosite–mangerite–charnockite–granite (AMCG) associations by claiming a common mantle progenitor and fractionation history for all the rock-types (e.g. Turner *et al.*, 1992). Rather extensive dike swarms of tholeiitic diabase and quartz–feldspar porphyry are also known, but volcanic rocks are sparse (Rämö & Haapala, 2005; Rämö *et al.*, 2009). A distinct feature of the classic Finnish rapakivi association compared with other corresponding occurrences, for example those in the Grenville province of Canada, is that mafic rocks are fairly uncommon (e.g. Ashwal, 1993).

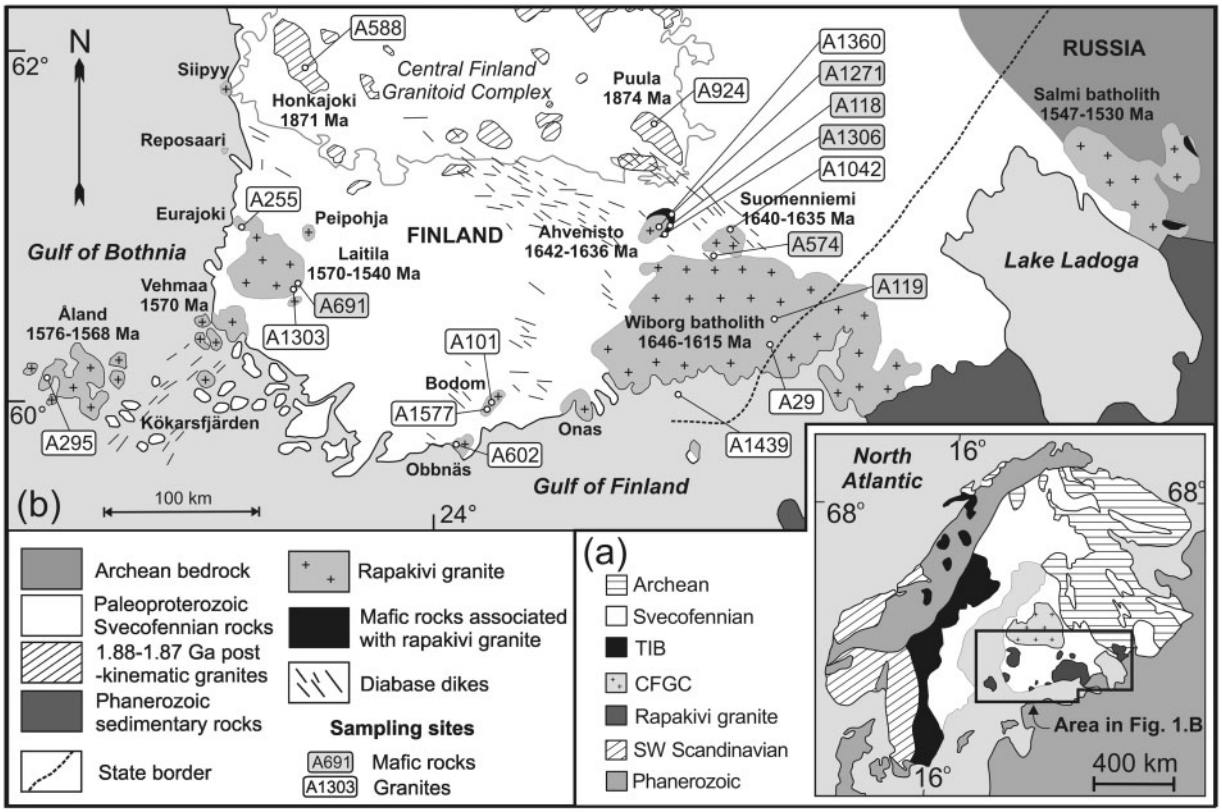

Fig. 1. Map of the study area. (a) Location of the study area on the Fennoscandian Shield relative to the main crustal domains (modified after Högdahl *et al.*, 2004; Rämö & Haapala, 2005; Andersen *et al.*, 2009). (b) Map of the Finnish rapakivi area and sample locations (modified after Elliott, 2003; Rämö & Haapala, 2005). TIB, Transscandinavian Igneous Belt.

REGIONAL GEOLOGY AND SAMPLING

The samples were chosen from representative rock types of the Finnish rapakivi province to obtain a sufficient temporal and geographical coverage of samples previously studied with other isotope methods. Background information with references to sample locations, ages and whole-rock Nd and zircon O isotope compositions is provided in Table 1. Brief petrographic descriptions of the samples are given in Table 2.

Wiborg batholith

The largest (~19 000 km^2) rapakivi intrusion in Finland is the 1646–1615 Ma (Rämö & Haapala, 2005) Wiborg batholith, partially located in Russia. The lithology of the batholith is diverse, but most of it comprises wiborgite, the rapakivi granite proper (see Vorma, 1976; Haapala & Rämö, 1992). Some gabbro–anorthositic rocks are found as minor inclusions, mostly in the east–central part of the batholith. Three rock types were sampled from the Wiborg batholith for this study. Sample A29 is from a typical wiborgite from the central part of the batholith. Sample A1493 was taken from the island of Ristisaari in the southern part of the Wiborg batholith (Gulf of Finland archipelago) and represents the dark varieties of wiborgitic rapakivi granites that include basic plagioclase megacrysts (xenocrysts) (Turkki, 2005). Sample A119 is an anorthosite from an anorthositic megaxenolith in the east–central part of the Wiborg batholith.

Suomenniemi intrusion

The ~365 km^2, ~1640 Ma (Vaasjoki *et al.*, 1991) Suomenniemi batholith is located on the northeastern flank of the Wiborg batholith and is lithologically diverse (Rämö, 1991). The bulk of the intrusion is formed of two mutually gradational granite types: an even-grained hornblende granite in the south grades to a dominant more evolved, coarse biotite granite in the north (Rämö, 1991). Sample A1042 is from the northern part of the intrusion.

Lovasjärvi mafic intrusion

The tholeiitic ~1643 Ma (Siivola, 1987) Lovasjärvi mafic intrusion, is located between and cut by the Suomenniemi and Wiborg batholiths (Fig. 1b). The intrusion consists of two parts: a concentric melatroctolite–olivine gabbro

Table 1: Locations, U–Pb TIMS ages, whole-rock Nd, and zircon O isotope compositions of the samples, with references to original studies

Sample Rock type	Pluton	Co-ordinates*		Age (Ma)	ε_{Nd}††	$\delta^{18}O$‡
		x	*y*			
Younger age group						
Rapakivi granites						
A255 fayalite–hornblende granite	Eurajoki	6787000	1533600	1571 ± 3[1]	$-2{\cdot}2$[4]	8·5
A295 biotite–hornblende granite	Åland	6677970	1420860	1575 ± 11[2]	$-1{\cdot}4$[10]	6·1
A1303 biotite granite	Kolinummi	6746940	1571000	1576 ± 3[1]	$-2{\cdot}6$[4]	8·8
Leucogabbronorite						
A691 leucogabbronorite	Kolinummi	6744000	1570000	1584 ± 2[3]	$-1{\cdot}6$[10]	7·6
Older age group						
Rapakivi granites						
A1493 hornblende granite	Wiborg	6689200	3489250	1627 ± 3[4]	$-1{\cdot}3$[4]	n.a.
A1360 biotite granite	Ahvenisto	6799000	3476300	1633 ± 6[5]	$-2{\cdot}3$[11]	8·1
A29 biotite–hornblende granite	Wiborg	6725400	3547600	1633 ± 5[2]	$-1{\cdot}2$[10]	7·2
A1577 biotite granite	Bodom	6684900	2542500	1638 ± 2[6]	$-1{\cdot}0$[12]	6·2
A1042 biotite granite	Suomenniemi	6803950	3519310	1639 ± 6[7]	$-2{\cdot}2$[10]	8·1
A602 hornblende granite	Obbnäs	6659640	2520910	1640 ± 14[6]	$-1{\cdot}9$[13]	6·2
A101 biotite granite	Bodom	6689000	2544000	1645 ± 12[3]	n.a.	n.a.
Mafic and intermediate rocks						
A1306 quartz monzodiorite	Ahvenisto	6794100	3478050	1642 ± 2[5]	$-1{\cdot}1$[11]	7·0
A119 anorthosite	Wiborg	6740200	3546500	1633 ± 2[2]	$-1{\cdot}7$[4]	6·7
A1271 gabbroic pegmatite	Ahvenisto	6806440	3482380	1638 ± 6[5]	$+0{\cdot}5$[11]	n.a.
A118 leucogabbronorite	Ahvenisto	6797400	3480600	1643 ± 3[5]	$-0{\cdot}6$[11]	7·2
A574 diabase	Lovasjärvi	6782980	3507920	1643 ± 5[8]	$-0{\cdot}6$[14]	5·5
Svecofennian post-kinematic granites						
A588 biotite granite	Honkajoki	6905242	3252482	1871 ± 15[9]	$+0{\cdot}5$[9]	5·5
A924 porphyritic granite	Puula	6860700	3486800	1874 ± 4[9]	$-0{\cdot}5$[9]	7·8

*Co-ordinates in Finnish National Reference Grid.
†$(^{143}Nd/^{144}Nd)^0_{CHUR} = 0{\cdot}512638$ and $(^{147}Sm/^{144}Nd)^0_{CHUR} = 0{\cdot}1966$, $\lambda = 6{\cdot}54 \times 10^{-12}\,a^{-1}$.
‡Oxygen isotope data from Elliott *et al*. (2005).
References: [1]M. Vaasjoki & O. T. Rämö (unpublished data); [2]Suominen (1991); [3]Vaasjoki (1977); [4]O. T. Rämö (unpublished data); [5]Alviola *et al*. (1999); [6]P. Kosunen *et al*. (unpublished data); [7]Vaasjoki *et al*. (1991); [8]Siivola (1987); [9]Rämö *et al*. (2001); [10]Rämö (1991); [11]O. T. Rämö & M. Vaasjoki (unpublished data); [12]sample 333-JVK of Kosunen (2004); [13]sample 243-JVK of Kosunen (2004); [14]sample A1069 of Rämö (1991).

phase in the north and a gabbroic main phase in the south (Alviola, 1981). Sample A574 is from the main (gabbro) part of the intrusion.

Ahvenisto complex

The 350 km^2 Ahvenisto complex is the prominent occurrence of rapakivi-associated gabbro–anorthositic and monzodioritic rocks in Finland (e.g. Rämö & Haapala, 2005). The ~1640 Ma (Alviola *et al*., 1999; Heinonen *et al*., 2010) intrusion is located on the northwestern flank of the Wiborg batholith (Fig. 1) and comprises coeval granitic (70%; fraction at the current erosional level), gabbroic (25%, mostly leucogabbronoritic), and monzodioritic (5%) rocks. Four samples were taken from the main rock types of the complex. Sample A1360 is from the main granite phase. Sample A1306 is a quartz monzodiorite from the south–central part of a monzodioritic ring-dike that flanks the complex in the east (Alviola *et al*., 1999). The leucogabbronorite sample A118 represents the principal gabbro–anorthositic rock of the southeastern part of the complex and sample A1271 is from a coarse (c. 5 cm long) zircon crystal in a pegmatite pocket of a leucotroctolite in the northeastern part (Alviola *et al*., 1999).

Table 2: Petrographic summary of the studied samples

Sample	Rock type	Color	Grain size and texture	Main minerals	Accessory minerals	Remarks
Younger age group						
Rapakivi granites						
A255	hbl granite			afs, q, plag(An15–25), hbl & bt	ol, ap, zir & op	
A295	bt–hbl granite	deep red	medium- to coarse-grained, slightly porphyritic	q, afs, bt & hbl	zir, ap, fl & op	q & afs strongly granophyric
A1303	bt granite	greyish	coarse-grained, weakly porphyric	plag, afs, bt, amph, ol & q	ap, zir & op	ol altered, q mainly in groundmass
Leucogabbronorite						
A691	leucogabbronorite	dark grey	coarse-grained	plag, px & afs	ap, op & zir	secondary bt & chl
Older age group						
Rapakivi granites						
A1493	hbl granite	dark red	coarse-grained, rapakivi texture	afs, plag, q, hbl & bt	ol, zir, ap & fl	secondary chl & op
A1360	hbl–bt granite	light brown	coarse-grained	afsp, q, plag, bt & hbl	ap, fl, zir & op	mafic minerals as aggregates, secondary grun
A29	bt–hbl granite	dark red	coarse-grained, rapakivi texture	q, afs, plag, hbl & bt	zir, ap & op	
A1577	bt granite	red	medium- & even-grained, local rapakivi texture	afs, q, plag, bt & hbl	fl, all, zir, ap & op	secondary ser, musc, chl & ep
A1042	bt granite	reddish	coarse-grained, locally afs porphyric	afs, q, plag & bt	fl & zir	secondary amph
A602	hbl–bt granite	red	coarse-grained, afs porphyric	afs, q, plag(An_{23-27}), bt & hbl	sph, all, fl, zir, ap & op carb; brittle deformation	secondary chl, ser, musc, ep,
A101	bt granite	reddish	medium- to coarse-grained, local rapakivi texture	afs, q, plag, bt & amph	fl, all, zir & ap	amph secondary
Mafic and intermediate rocks						
A1306	q monzodiorite	greyish	medium-grained, locally plag(An_{55-60}) porphyritic	plag(An_{30-40}), afs & opx	amph, ap, op, zir & badd	secondary biotite
A119	anorthosite	dark grey	coarse-grained	plag & px	op, q, afs & zir	
A1271	gabbro pegmatite	dark grey	medium- to coarse-grained, locally plag porphyritic	plag, ol, ilm, bt & hbl	opx, afs & q	zircon collected from a pegmatite pocket
A118	leucogabbronorite	dark grey	coarse-grained	plag(An_{55}), opx & cpx	bt, chl, op, ol, afs, q, ap, zir, badd & ilm	
A574	gabbro	dark	coarse-grained, porphyric, lineated	plag, cpx, bt & hbl	op & zir	mafic minerals as aggregates
Svecofennian post-kinematic granites						
A588	bt granite	red	coarse-grained	afs, q & plag	bt, fl, zir, ep, ap & op	
A924	bt granite	grey	coarse-grained, afs & plag porphyric	afs, plag, q & bt	hbl, ap & zir	

afsp, alkali feldspar; all, allanite; amph, amphibole; An, anorthite composition; ap, apatite; badd, baddeleyite; bt, biotite; carb, carbonate; chl, chlorine; cpx, clinopyroxene; ep, epidote; fl, fluorite; grun, grunerite; hbl, hornblende; ilm, ilmenite; musc, muscovite; ol, olivine; op, opaque minerals; opx, orthopyroxene; plag, plagioclase; px, pyroxenes; q, quartz; ser, sericite; zir, zircon.

Bodom intrusion

The ~60 km^2 Bodom intrusion comprises two roughly coeval (~1645 Ma; Kosunen, 2004) rapakivi granite types with distinct trace-element characteristics. A porphyritic variety is the dominant rock type, intruded by an even-grained variety in the southwestern part of the intrusion with a sharp contact (Kosunen, 2004). Both granite types were sampled for this study. Sample A1577 represents the even-grained variety from the western part of the intrusion and the sample A101 is taken from the porphyritic type.

Obbnäs intrusion

The ~1640 Ma Obbnäs intrusion (Kosunen, 2004) is composed of a homogeneous, coarse-grained porphyritic hornblende–biotite granite. The southwestern parts of the intrusion are more primitive than the northwestern parts (hornblende more abundant, rapakivi texture more pronounced). The Obbnäs intrusion differs from all the other Finnish rapakivi intrusions as it includes accessory titanite, which might indicate higher magmatic fO_2 (Kosunen, 2004). In this respect Obbnäs is similar to the Estonian rapakivi granites (e.g. Rämö *et al.*, 1996). Sample A602 comes from the hornblende–biotite granite of the Obbnäs intrusion.

Laitila batholith and Eurajoki stock

The ~1570 Ma (Vaasjoki, 1977) Laitila batholith is an ~1400 km^2 rapakivi intrusion on the southwestern coast of Finland comprising a series of biotite–hornblende to biotite granites. On the southeastern flank of the batholith there is a small, separate anorthositic intrusion (Kolinummi). The ~1570 Ma (Vaasjoki, 1977) Eurajoki stock is a relatively small (~8 km^2) intrusion (Haapala, 1977) on the northwestern flank of the Laitila batholith and consists of (± olivine–)biotite–hornblende granites and topaz granites. Three samples were taken from these rocks. Sample 1303 is a biotite granite and A691 a leucogabbronorite from the Kolinummi intrusion. Sample A255 is a fayalite–hornblende granite from the marginal phase of the Eurajoki stock.

Åland (or Ahvenanmaa) batholith

The ~1570 Ma Åland batholith (Suominen, 1991) is the second largest rapakivi intrusion in Finland and covers ~5000 km^2 in the archipelago of southwestern Finland (Fig. 1). The prevailing rock type is a hornblende granite, which is cut by a more evolved biotite granite and some minor aplitic granites (Bergman, 1986). Sample A295 is from the southern part of the batholith and represents the main rock type of the batholith.

Svecofennian post-kinematic Honkajoki and Puula plutons

We have also included samples from the A-type synorogenic, post-kinematic granites from the Central Finland Granitoid Complex (CFGC) (Fig. 1). These are (in terms of geochemistry) similar to the rapakivi granites and serve to characterize the Lu–Hf isotope systematics of the lower parts of the Svecofennian crust in Finland (see Rämö *et al.*, 2001; Elliott, 2003). The Honkajoki and Puula plutons (1871 Ma and 1874 Ma, respectively; Rämö *et al.*, 2001) are Type 2 synorogenic, post-kinematic granites (Elliott, 2003) of the CFGC. The ~500 km^2 Honkajoki pluton is a multiphase intrusion in the western part of the CFGC (Fig. 1b) and comprises different types of hornblende–biotite granite and a coarse-grained biotite granite, and is associated with several separate mafic intrusions (Rämö *et al.*, 2001). The ~450 km^2 Puula pluton is located in the southeastern part of the CFGC (Fig. 1b) and is a more homogeneous intrusion dominated by an alkali feldspar and plagioclase-phyric monzogranite with occasional rapakivi texture. One sample from each of the plutons was analyzed: A588 from the main biotite granite of the Honkajoki pluton and A924, the monzogranite of the Puula pluton.

ANALYTICAL METHODS

Clear, non-metamict and inclusion-free zircon grains were hand-picked from pure, non-magnetic zircon fractions produced by standard mineral separation methods (Wilfley-table, heavy liquid and magnetic separation). The selected grains were cast in epoxy and polished for analysis. Imaging by cathodoluminescence and backscattered electrons was carried out with a JEOL JSM-6460LV scanning electron microscope at the Department of Geosciences, University of Oslo. LAM-ICP-MS Lu–Hf isotope analysis was performed using a Nu Plasma HR multicollector ICP-MS system with a U–Pb collector block and a New Wave/Merchantek LUV-213 Nd:YAG laser microprobe, also at the Department of Geosciences, University of Oslo. Trace elements in zircon were analysed by laser ablation quadrupole (LAQ)-ICP-MS using an Agilent 7500 system with a New Wave LUV213 laser microprobe at the Department of Geology, University of Helsinki.

LAM-ICP-MS analysis of Lu–Hf isotopes

Masses 172–179 were measured simultaneously in Faraday collectors. Ablation was conducted in helium, at the following conditions: beam diameter 55 μm (aperture imaging mode); pulse frequency 5 Hz; beam fluence *c.* 2 J/cm^2, static ablation. Each ablation was preceded by a 30 s on-mass background measurement. The total Hf signal obtained was in the range 1·5–3·0 V. Under these conditions, 120–150 s of ablation was required to obtain an internal precision of ≤ ±0·000020 (1SE).

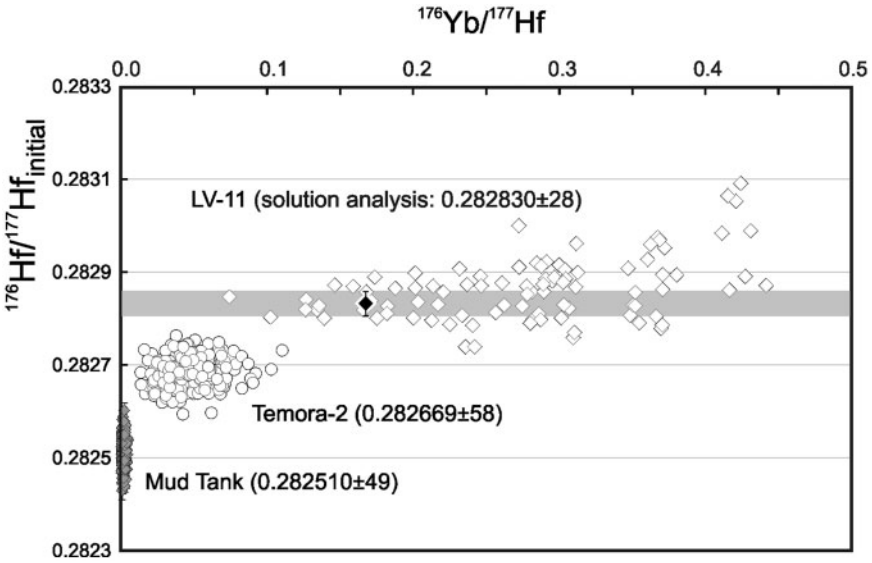

Fig. 2. LAM-ICP-MS (open symbols) and solution ICP-MS (LV-11, single filled diamond with error bars and the shaded bar) data on Lu–Hf reference samples. The numbers given are average $^{176}Hf/^{177}Hf$ with ± 2SD in the last two significant decimal places at the age of crystallization of the zircon (732 Ma for Mud Tank, 414 Ma for Temora-2, 290 Ma for LV-11). LV-11 is a single zircon crystal from a nepheline syenite pegmatite in the Oslo Rift, Norway, which has been used to tune the Yb interference correction at mass 176. The crystal is zoned in REE/Hf, but has a constant $^{176}Hf/^{177}Hf$.

Isotope ratios were calculated using the Nu Plasma time-resolved analysis software. The raw data were corrected for mass discrimination using an exponential law, the mass discrimination factor for Hf was determined assuming $^{179}Hf/^{177}Hf = 0{\cdot}7325$, and the observed 2 SE uncertainty of the Hf mass discrimination factor was better than 0·5%, which was propagated through to the error of the final result. The mass discrimination factor for Yb was monitored from the $^{173}Yb/^{172}Yb$ ratio, and depending on the Yb content of the zircon, it could be determined with an internal precision (2SE) one to two orders of magnitude worse than that for Hf, which is insufficient for use in the isobaric overlap correction procedure at mass 176. The correction for ^{176}Yb interference was therefore made by the procedure described by Andersen *et al.* (2009), using multiple LAM-ICP-MS analyses of zircon with constant $^{176}Hf/^{177}Hf$ but variable Yb/Hf ratio to determine the $^{176}Yb/^{172}Yb$ ratio to be used in the overlap correction. However, some samples in this study have maximum $^{176}Yb/^{177}Hf$ ratios significantly exceeding the maximum value of the Temora-2 reference zircon (*c.* 0·12). To better control the Yb correction for high Yb/Hf zircons, we have therefore tuned the correction parameters from multiple LAM-ICP-MS analyses of zircon LV-11, which is a *c.* 10 mm euhedral crystal from the nepheline syenite pegmatite at Låven island in the Oslo Rift (290 Ma, source: mineralogical collection of the Natural History Museum, University of Oslo).

Solution analysis of the LV-II zircon using a Nu Plasma mass spectrometer at GEMOC, Macqurie University, Australia gave $^{176}Hf/^{177}Hf = 0{\cdot}282837 \pm 0{\cdot}000028$ at $^{176}Lu/^{177}Hf = 0{\cdot}0026 \pm 0{\cdot}0002$ and $^{176}Yb/^{177}Hf = 0{\cdot}166 \pm 0{\cdot}011$, corresponding to an initial $^{176}Hf/^{177}Hf$ at 290 Ma of $0{\cdot}28283 \pm 0{\cdot}00003$ (mean of three analyses, J. Payne, personal communication). Multiple LAM-ICP-MS analyses of the zircon made at GEMOC and in Oslo indicate that the crystal has a range of $^{176}Yb/^{177}Hf$ from 0·075 to 0·45 (Fig. 2). Iteratively adjusting the $^{176}Yb/^{172}Yb$ ratio to obtain an optimal fit between laser ablation and solution analyses gives an adjusted $^{176}Yb/^{172}Yb = 0{\cdot}58747$, which is near the average of published isotope ratios for natural Yb (Chu *et al.*, 2002; Segal *et al.*, 2003).

$^{176}Lu/^{175}Lu = 0{\cdot}02669$ was used for correction of Lu interference on mass 176 (DeBievre & Taylor, 1993). Based on this revised correction, Temora-2 gives present-day $^{176}Hf/^{177}Hf = 0{\cdot}282669 \pm 58$ (2SD, $n = 337$), which can be compared with the solution analysis at $0{\cdot}282686 \pm 8$ published by Woodhead & Hergt (2005). The low-REE Mud Tank reference zircon gave $^{176}Hf/^{177}Hf = 0{\cdot}282510 \pm 49$ (2SD, $n = 817$), which is indistinguishable from the solution analysis at $0{\cdot}282507 \pm 6$ of Woodhead & Hergt (2005).

A value for the decay constant of ^{176}Lu of $1{\cdot}867 \times 10^{-11}\,a^{-1}$ has been used in all calculations (Scherer *et al.*, 2001, 2007; Söderlund *et al.*, 2004). For the calculation of ε_{Hf} values we use present-day chondritic $^{176}Hf/^{177}Hf = 0{\cdot}282785$ and $^{176}Lu/^{177}Hf = 0{\cdot}0336$ (Bouvier *et al.*, 2008). We have adopted the depleted mantle model of Griffin *et al.* (2000), modified to the λ ^{176}Lu and chondritic composition used, which produces a present-day value of $^{176}Hf/^{177}Hf$ (0·28325, $\varepsilon_{Hf} = +16.4$) similar to that of average mid-ocean

Table 3: LAQ-ICP-MS trace element analysis conditions and standard compositions

	Mass	Dwelltime (ms)	NBS612* (ppm)	GJ-1 reference zircon (yellowish brown)					
				n	Average	2SD (ppm)	2SE	2RSD (%)	2RSE (%)
Si	29	10	336600		153200	*Internal standard*			
Ti	49	50	44	9	4·3	0·5	0·2	13	4·2
Y	89	50	38	34	228	41	7	18	3·1
Nb	93	50	40	16	1·6	0·3	0·1	19	4·7
La	139	50	35·8	34	0·006	0·008	0·001	135	23·2
Ce	140	50	38·7	34	14·3	2·5	0·4	18	3
Pr	141	50	37·2	34	0·029	0·006	0·001	22	3·8
Nd	146	50	35·9	34	0·62	0·13	0·02	21	3·5
Sm	147	50	38·1	34	1·52	0·22	0·04	14	2·5
Eu	153	50	35	34	0·95	0·13	0·02	14	2·4
Gd	157	50	36·7	34	6·3	1·37	0·23	22	3·7
Tb	159	50	36	34	1·81	0·24	0·04	13	2·3
Dy	163	50	36	34	20	2·7	0·5	14	2·3
Ho	165	50	38	34	6·5	1·0	0·2	15	2·6
Er	166	50	38	34	29·0	4·9	0·8	17	2·9
Tm	169	50	38	34	6·8	0·9	0·1	13	2·2
Yb	172	50	39·2	34	68·7	9·9	1·7	14	2·5
Lu	175	50	36·9	34	11·3	2·7	0·5	24	4·2
Hf	178	50	35	34	6341	1825	313	29	4·9
Ta	181	50	40	16	0·45	0·12	0·03	27	6·7
Pb	208	50	38·57	16	0·57	0·25	0·06	44	11
Th	232	50	37·79	34	10·3	2·5	0·4	25	4·2
U	238	50	37·38	34	217	39	7	18	3·1

*Source of standard values: GeoRem database (Max Planck Institut für Chemie, Mainz, Germany), 'preferred values', December 2008.

ridge basalt (MORB) over 4·56 Ga, from chondritic initial hafnium at $^{176}Lu/^{177}Hf_{DM} = 0{\cdot}0388$.

Standards or reference zircons 91500, Temora-2, Mud Tank and GJ-1 were run as unknowns at frequent intervals. Data obtained over a 2 year period indicate an accuracy within $\leq \pm 0{\cdot}000020$; the observed external reproducibility on Temora-2 of $\pm 0{\cdot}000058$ (2SD, Fig. 2) gives a conservative estimate of an uncertainty of ± 2 ε units.

LAQ-ICP-MS analysis of trace elements

Analyses were made in time-resolved mode in which a 30 s on-peak background measurement with the laser off was followed by 90 s of ablation. The laser conditions used were: spot size 40–100 μm; repetition rate 10 Hz; fluence 2–3 J/cm^2 (45% energy output). The masses measured per cycle and the dwell-time per mass are given in Table 3. NIST612 was used as an external standard; the elemental concentrations used are given in Table 3. Si was used as an internal standard, assuming stoichiometric composition of zircon with 32.78 wt % SiO_2 (153 200 ppm).

Data reduction was performed off-line, using the Agilent ChemStation time-resolved analysis software and a Microsoft Excel2003/VBA spreadsheet program, which allowed the interactive selection of homogeneous parts of the signals for integration. The results of repeated analyses of a yellowish brown crystal of the GJ-1 reference sample (provided by Dr. E. A. Belousova, Macquarie University, NSW, Australia) are given in Table 3. The REE were determined with an external 2SD precision in the range 13–20%, with the exception of La (135%) and Pr, Nd, Gd and Lu (≤25%). The cause for the large analytical uncertainty for La is the low concentration in zircon (≪1 ppm); repeated analyses of NBS612 run as an unknown suggest that at higher concentrations, the uncertainty in La is comparable with that of the other REE.

Table 4: Summary of the Lu–Hf isotope results

Sample	*n*	Measured isotope ratios								Initial isotope values			
		$^{176}Hf/^{177}Hf$	±2SD	$^{178}Hf/^{177}Hf$	±2SD	$^{176}Lu/^{177}Hf$	±2SD	$^{176}Yb/^{177}Hf$	±2SD	$^{176}Hf/^{177}Hf$	±2SD	ε_{Hf}	±2SD
Younger age group													
Rapakivi granites													
A255	20	0·281749	0·00003	1·467251	0·00007	0·000846	0·00029	0·028633	0·0105	0·281724	0·000032	−2·2	1·2
A295	24	0·281804	0·00005	1·467275	0·00009	0·000597	0·00046	0·023482	0·0205	0·281786	0·000053	+0·1	1·9
A1303	27	0·281779	0·00004	1·467240	0·00009	0·000529	0·00023	0·019559	0·0088	0·281763	0·000038	−0·7	1·3
Leucogabbronorite													
A691	20	0·281894	0·00014	1·467269	0·00009	0·001378	0·00092	0·071763	0·0529	0·281853	0·000128	+2·7	4·6
Older age group													
Rapakivi granites													
A1493	26	0·281762	0·00005	1·467255	0·00012	0·000558	0·00028	0·021267	0·0137	0·281745	0·000047	−0·1	1·7
A1360	25	0·281756	0·00006	1·467303	0·00011	0·000566	0·00029	0·027383	0·0145	0·281738	0·000056	−0·2	2·0
A29	23	0·281788	0·00009	1·467263	0·00012	0·000935	0·00142	0·044356	0·0761	0·281759	0·000070	+0·5	2·5
A1577	24	0·281787	0·00006	1·467296	0·00008	0·000609	0·00043	0·031129	0·0226	0·281769	0·000055	+1·0	2·0
A1042	45	0·281777	0·00009	1·467265	0·00010	0·001417	0·00208	0·065544	0·0990	0·281733	0·000077	−0·3	2·7
A602	39	0·281748	0·00007	1·467265	0·00008	0·000533	0·00077	0·021926	0·0347	0·281732	0·000062	−0·3	2·2
A101	12	0·281781	0·00005	1·467287	0·00011	0·000758	0·00062	0·036721	0·0320	0·281757	0·000037	+0·7	1·3
Mafic rocks													
A1306	16	0·281814	0·00007	1·467263	0·00010	0·000989	0·00059	0·043461	0·0280	0·281783	0·000064	+1·6	2·3
A119	20	0·281852	0·00014	1·467283	0·00011	0·001143	0·00103	0·057211	0·0516	0·281816	0·000109	+2·5	3·9
A1271	53	0·281793	0·00008	1·467269	0·00009	0·001054	0·00066	0·063499	0·0426	0·281760	0·000077	+0·7	2·7
A118	19	0·281863	0·00013	1·467273	0·00011	0·001228	0·00088	0·057897	0·0402	0·281825	0·000109	+3·1	3·9
A574	31	0·281924	0·00017	1·467285	0·00011	0·002027	0·00146	0·105160	0·0730	0·281860	0·000132	+4·3	4·7
Svecofennian post-kinematic granites													
A588	35	0·281659	0·00006	1·467256	0·00012	0·001195	0·00098	0·050852	0·04480	0·281617	0·000060	0·9	2·0
A924	41	0·281637	0·00008	1·467259	0·00008	0·000869	0·00064	0·035335	0·02833	0·281606	0·000080	0·6	2·7

n, number of analyses used in calculation of the average values. 2SD values given do not refer to propagated error estimates of the original analysis, but to the observed variation of isotope compositions of different zircon grains within single samples.

HAFNIUM ISOTOPE COMPOSITION OF ZIRCON

The average values for the measured $^{176}Lu/^{177}Hf$, $^{176}Yb/^{177}Hf$ and $^{176}Hf/^{177}Hf$ in zircon with calculated initial $^{176}Hf/^{177}Hf$ isotope ratios and corresponding initial ε_{Hf} values are summarized in Table 4. Initial $^{176}Hf/^{177}Hf$ ratios were calculated to the U–Pb ID-TIMS ages of the samples (Table 1). The analysis results are also presented on isochron diagrams in Fig. 3, on $^{176}Yb/^{177}Hf$ vs initial $^{176}Hf/^{177}Hf$ diagram in Fig. 4, and on an age vs initial $^{176}Hf/^{177}Hf$ diagram in Fig. 5. The Lu–Hf isotope data are available in Electronic Appendix 1 (available for downloading at http://www.petrology.oxfordjournals.org/).

The extreme values of REE/Hf in the analyses are higher than what is commonly observed in zircons from granitic systems, with maximum $^{176}Lu/^{177}Hf$ of 0·005 (Table 4, Fig. 3) and $^{176}Yb/^{177}Hf$ ranging to >0·21. The majority of zircons, however, have REE/Hf ratios well below these maximum values, with $^{176}Lu/^{177}Hf \leq 0{\cdot}002$ and $^{176}Yb/^{177}Hf \leq 0{\cdot}1$. For zircon from the granitic rocks, the present-day variation in $^{176}Hf/^{177}Hf$ is correlated with $^{176}Lu/^{177}Hf$, suggesting that the variation in Hf isotopic composition in these samples is entirely due to *in situ* accumulation of radiogenic ^{176}Hf (Fig. 3). This is also true for zircon from the Svecofennian Honkajoki and Puula granites (Fig. 3e). The scatter around the visual best-fit reference lines can largely be accounted for by analytical error (i.e. ±0·00006). Zircons from gabbro (samples A574 and A1271), leucogabbronorite (A118 and A691), and anorthosite (A119) show larger ranges in Hf isotope composition (Figs 3 and 4), significantly exceeding the expected analytical error. In these samples, $^{176}Hf/^{177}Hf$ is still correlated with $^{176}Lu/^{177}Hf$ (Fig. 3) and also with $^{176}Yb/^{177}Hf$ (Fig. 4),

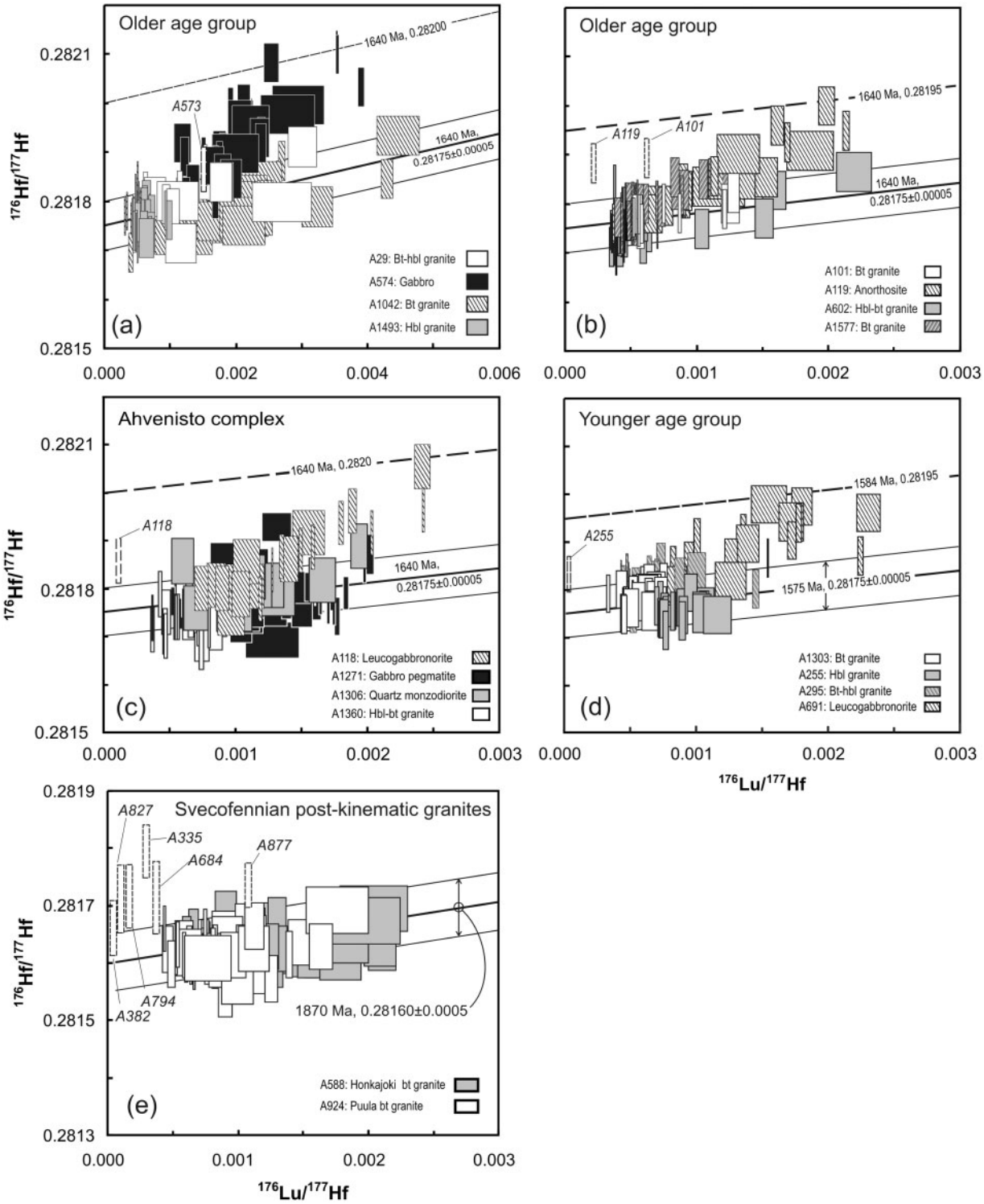

Fig. 3. Lu–Hf isochron diagrams for the studied samples. Also included are bulk-zircon ID-TIMS results from Patchett *et al.* (1981), and error boxes with dashed outlines denoting ±2SD.

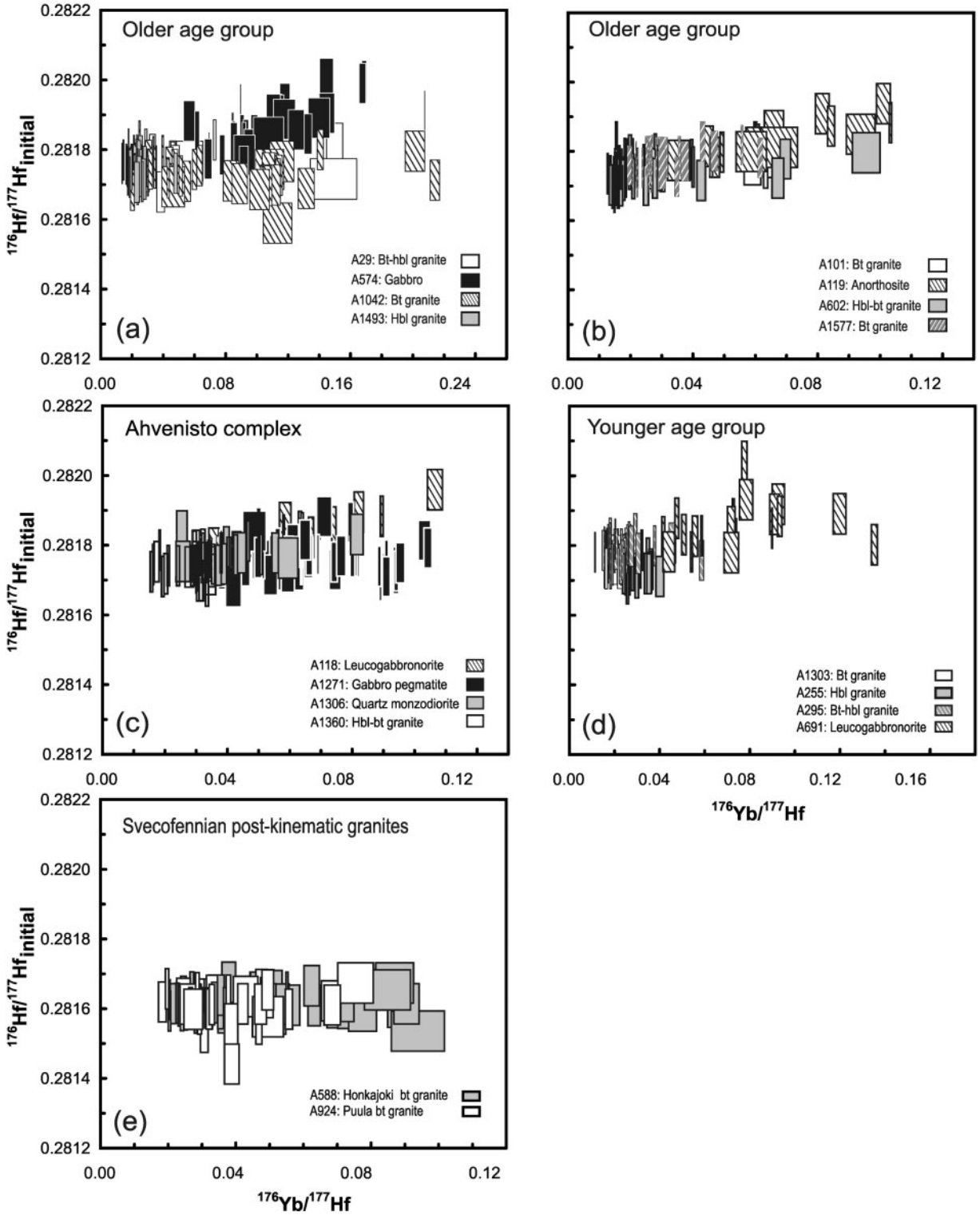

Fig. 4. Measured $^{176}Yb/^{177}Hf$ vs initial $^{176}Hf/^{177}Hf$ compositions of the studied samples. Error boxes denote ±2SD.

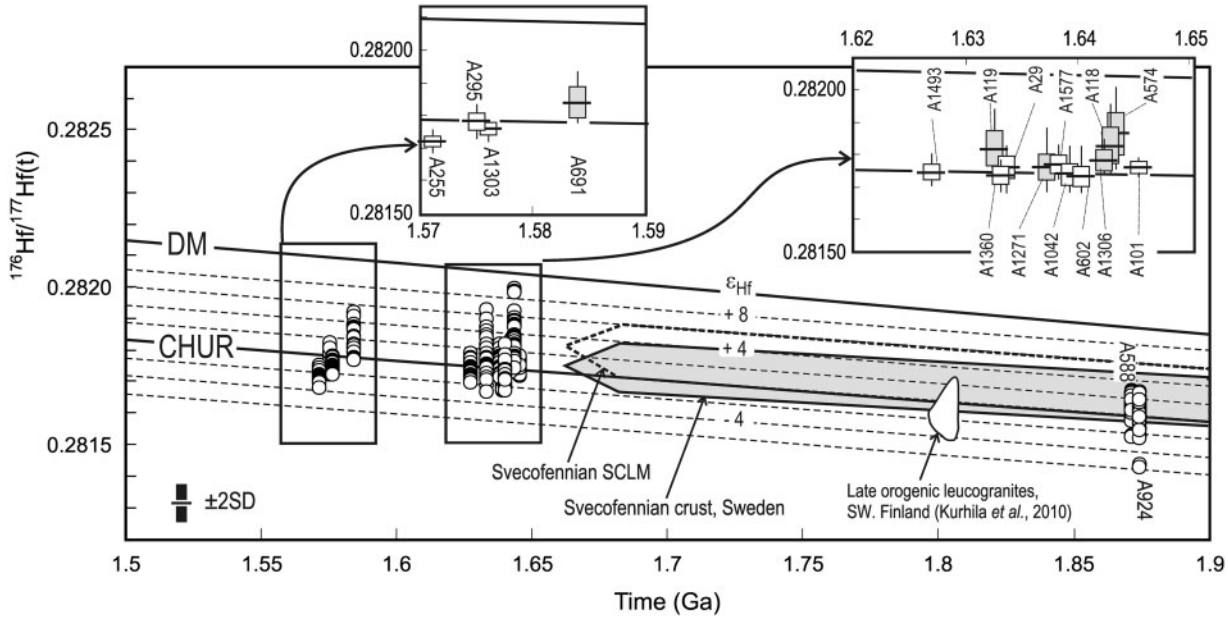

Fig. 5. Samples plotted on an initial Hf isotope composition vs age diagram. The shaded arrow depicting the Hf evolution of the Swedish Svecofennian crust and the arrow with the dashed line depicting the Fennoscandian sub-lithospheric mantle are shown according to Andersen *et al.* (2009).

but along trends that are too steep to be accounted for by *in situ* radiogenic growth alone.

Recalculated to the U–Pb ID-TIMS ages of the single intrusions (Table 1), the initial $^{176}Hf/^{177}Hf$ of zircon from the granitic rocks straddle the CHUR growth curve ($\varepsilon_{Hf} \sim -4$ to $+4$, Table 4, Fig. 5). These zircons also generally overlap with the trend of primitive Svecofennian crust suggested as a source for the granitic magmas of the Transscandinavian Igneous Belt (TIB) by Andersen *et al.* (2009). The initial $^{176}Hf/^{177}Hf$ of zircon from gabbro, leucogabbronorite and anorthosite ranges to higher maximum values, $\varepsilon_{Hf} \sim +6$ in the younger age group and $\varepsilon_{Hf} > +8$ in the Ahvenisto complex (Fig. 5). The initial $^{176}Hf/^{177}Hf$ of zircons from the Honkajoki and Puula granites also straddle the CHUR curve, and most zircons fall within the range of the source of TIB magmas at 1·87 Ga. Some zircons from these intrusions fall below this range. A similar pattern of Hf composition has been observed in the Svecofennian Perniö and Jaani leucogranite intrusions (Kurhila *et al.*, 2010).

TRACE ELEMENT COMPOSITION OF ZIRCON

Zircons from two representative samples [gabbro A574, which has the greatest initial Hf isotope variation (~9 ε_{Hf} units), and biotite granite Al042 (within-sample variation of ~5 ε_{Hf} units)] were analyzed for their trace element contents to examine the relations between elemental compositional variations and Hf isotope composition. Where possible, trace element and Hf isotope data were collected from the same portions of the zircon grains. The results are given in Tables 5 and 6 and are displayed on chondrite-normalized multi-element variation diagrams in Fig. 6. The data are also plotted on selected variation diagrams in Figs 7 and 8.

Most of the zircons in both samples show typical magmatic trace element patterns with high Hf, U, Th, Y and heavy REE (HREE) levels, relative enrichment of HREE over LREE, and moderate to strong negative Eu anomalies (Eu/Eu* from 0·01 to 0·5) in all analyses except in one (A574-25). The Th/U ratios of the zircons from both samples are comparable, have typical magmatic values on average (1·12 in Al042 and 1·32 in A574), but reach higher values in analyses from the gabbro (Th/U up to 2·7). The abundances of LREE vary considerably in both samples, with positive Ce anomalies (Ce/Ce* <30·8) in the zircons with low ('normal') LREE abundances.

High levels of LREE in zircon can be attributed to metamictization (Belousova *et al.*, 2002), hydrothermal alteration (Hoskin, 2005), or the effects of minute melt and mineral inclusions (Hoskin & Schaltegger, 2003). Only the clearest and colourless grains with magmatic features (definitive crystal faces) were selected; altered and featureless grain portions were avoided in the analyses. Thus it is most likely that the high LREE abundances evident in some of the analyses are affected by undetected submicroscopic mineral or melt inclusions in the zircon.

Table 5: Trace element composition of zircons in sample A1042

Grain:	1	2	3	4	5	6	7	14	18	22	23
P	562	107	8421	2212	133	189	310	112	342	128	251
Ti	53·9	12·9	55·9	23·0	56·2	23·5	136	24·5	29·2	36·8	198
Y	2479	604	1397	2230	1993	2900	2200	865	1658	1622	1159
Nb	10	5·6	21	13	4·4	15	21	7·3	7·9	4·0	25
La	4	0	500	640	3	3	7	3	17	5	50
Ce	17·5	6·94	968	1300	15·8	22·3	21·9	14·4	42·3	13·7	288
Pr	1·99	0·07	145	200	1·98	2·15	2·70	1·23	5·50	1·28	27·1
Nd	17·8	1·28	722	956	19·2	21·7	18·8	6·97	32·6	10·5	166
Sm	18·8	2·57	132	207	19·4	25·4	18·8	7·0	18·0	12·5	54·7
Eu	1·48	0·13	1·54	2·31	1·71	1·10	1·19	0·29	0·62	1·55	1·14
Gd	79·7	13·8	144	216	73·6	102	75·8	30·7	55·9	58·3	83·7
Tb	23·4	4·50	21·7	36·1	20·2	28·9	21·0	8·16	17·0	16·3	21·0
Dy	271	59·2	210	310	228	342	252	94·2	194	185	212
Ho	91·5	21·3	52·6	88·7	74·9	112	83·5	32·8	62·2	59·8	53·7
Er	376	101	212	342	310	465	356	153	271	259	222
Tm	73·6	22·5	42·8	68·3	60·8	96·6	70·2	32·7	57·9	51·3	48·3
Yb	594	210	329	567	498	837	581	293	500	440	422
Lu	105	31·5	57·7	85·5	85·4	119	98·8	43·6	72·1	75·0	52·5
Hf	10515	13419	11760	14173	13209	12544	11137	14194	13939	13249	10202
Ta	1	2	3	5	1	5	1	2	3	1	2
Pb	391	108	191	346	256	267	225	138	215	139	132
Th	116	47·2	92·3	247	73·5	241	100	74·6	125	57·4	125
U	86·8	67·6	81·2	225	52·7	198	102	79·1	114	43·8	116
$(Eu/Eu^*)_N$[1]	0·10	0·05	0·03	0·03	0·12	0·06	0·08	0·05	0·05	0·15	0·05
$(Ce/Ce^*)_N$[1]	1·42	20·50	0·86	0·87	1·42	2·12	1·19	1·86	1·05	1·31	1·85
Th/U	1·3	0·7	1·1	1·1	1·4	1·2	1·0	0·9	1·1	1·3	1·1
Nb/Ta	8·2	2·4	7·7	2·5	5·3	3·1	14·3	3·0	2·9	4·9	13·8
Yb/Sm	31·6	81·7	2·5	2·7	25·7	33·0	30·9	41·6	27·8	35·3	7·7
$(\Sigma REE + Y):P$[2]	2·1	2·8	0·1	0·8	7·2	7·5	3·4	3·9	2·4	6·2	2·9

Abundances are given in ppm. Av., average of two integrations.
[1]Normalized to chondritic values of McDonough & Sun (1995), calculated as $[Eu_N/(Sm_N + Gd_N)/2]$.
[2]Normalized to chondritic values of McDonough & Sun (1995), calculated as $[Ce_N/(La_N + Pr_N)/2]$.
[3]Ratio calculated for cationic REE, Y, and P.

Zircons from the biotite granite (A1042) have abundances of middle REE (MREE) to HREE that are comparable with average values of zircons from granitic rocks. In contrast, the zircons from the gabbro (A574) have considerably higher HREE than is found in zircon from most mafic rocks (e.g. Belousova *et al.*, 2002). It is possible that the exceptionally high contents of Y, Th, U, and to some extent Pb in gabbro A574 (Table 6, Fig. 7) could indicate early precipitation of zircon, possibly as a result of locally reached saturation conditions (Hoskin *et al.*, 2000; Hoskin & Schaltegger, 2003). However, lack of textural information precludes more detailed inferences of the timing of zircon saturation solely on the basis of these limited data.

The compositional peculiarities of the zircons from gabbro A574 are unprecedented and not fully understood. It is known, however, that the relatively high P content of the magma (1·07 wt% P_2O_5 in whole-rock A574) has provided sufficient pentavalent substitutes to account for some of the xenotime-type substitution required for incorporation of trivalent REE and Y. The abundances of REE and Y correlate with P, but the cationic $(\Sigma REE + Y):P$ ratios are relatively high in almost all analyses, reaching values as high as 7·5 in the granite (A1042) and 15·9 in the gabbro (A574). In some of the analyses the elevated LREE levels naturally affect these ratios and in general Y dominates them; nevertheless, a very complex

Table 6: Trace element composition of zircons in sample A574

Grain:	1	2	3	6av.	7	9	10	11	12	13	14	15	16	18	19	20av.	23	25	26	27	28	29	30
P	270	433	234	278	204	403	95·8	257	233	295	178	277	218	316	201	249	387	191	339	304	152	223	143
Ti	13·1	40·7	37·1	27·5	30·5	25·4	113	40·8	20·0	21·7	12·6	18·6	108	24·2	33·2	14·7	107	18·6	47·5	64·7	19·5	21·3	7·22
Y	6258	11082	4793	6375	4966	9459	1429	5525	5511	7068	2973	4414	5975	9081	4170	4081	8523	2020	5463	4723	1127	3507	2137
Nb	15	12	2·3	9·4	4·3	14	1·6	4·2	3·7	21	3·1	10	4·7	13	4·3	7·7	32	11	4·3	4·2	0·7	2·1	0·6
La	2	76	2	720	230	1	25	78	77	270	18	0	100	320	140	53	57	26	96	3	1	3	1
Ce	61·3	223	33·3	1710	383	116	87·9	132	202	515	95·2	89·1	466	1140	493	206	203	99·2	490	60·4	17·7	39·7	22·3
Pr	1·0	24	2·7	193	59	2·2	13	11	23	51	11	0·7	80	190	85	30	10	8·0	73	2·3	0·9	2·7	0·5
Nd	11	130	31	770	330	29	77	60	110	240	81	11	540	1270	543	192	57	52	469	23	7	24	6
Sm	23·6	61·8	33·2	130	105	49·9	30·4	34·6	53·1	54·5	37·4	21·5	233	396	183	62	41	15	149	28	7	25	11
Eu	0·8	4·6	1·4	18	14	1·3	3·9	13	3·2	6·2	3·6	0·3	33	36	32	5·0	7·3	11	26	0·8	0·5	1·1	0·6
Gd	150	240	130	270	200	270	59	160	180	190	100	110	330	490	240	140	200	40	200	120	28	100	51
Tb	49·5	79·1	41·9	69·2	53·0	86·6	15·6	50·4	51·8	61·3	30·1	35·9	77·2	101	51·3	40·9	66·6	14·3	50·4	37·4	9·22	33·7	17·9
Dy	639	1030	517	778	608	1070	175	640	623	755	362	458	807	1040	533	483	862	194	585	461	120	415	235
Ho	213	374	180	253	197	356	56·9	217	206	250	118	156	240	322	164	147	288	66·5	193	161	41·1	135	79·0
Er	909	1730	791	1060	837	1480	242	925	869	1060	495	687	956	1330	678	558	1260	293	807	697	176	560	338
Tm	192	346	163	221	177	305	51·3	194	187	231	108	154	190	273	141	112	271	65·8	159	139	37·5	112	70·8
Yb	1570	2690	1310	1870	1510	2460	444	1560	1590	2020	940	1360	1500	2340	1200	912	2260	562	1230	1100	308	897	582
Lu	187	448	191	248	199	305	61·4	218	210	248	124	174	185	319	159	117	277	73·2	183	183	40·6	119	76·9
Hf	13878	12699	12554	10067	12433	12881	7823	9324	13494	17605	12812	16013	12564	12810	12530	8074	14622	10520	10411	9910	7083	7027	8113
Ta	13	7	3	6	4	7	1	4	3	13	2	9	3	5	3	6	26	11	3	2	1	1	0
Pb	2140	3682	1204	2020	1563	2925	381	2516	1519	2008	1419	2439	2605	2661	1384	1009	3406	1915	1855	1852	3623	1400	1271
Th	3185	3713	715	1618	1061	4024	203	3737	1473	3164	858	5366	2084	3907	918	2058	6051	970	1714	1610	1572	867	1365
U	1778	2889	867	1825	1330	2371	274	1872	1233	1822	1087	1965	1899	2163	1134	846	3025	1470	1342	1265	2824	1120	1044
$(Eu/Eu^*)_N$[1]	0·03	0·10	0·06	0·29	0·29	0·03	0·28	0·45	0·09	0·17	0·17	0·01	0·37	0·25	0·46	0·16	0·20	1·29	0·47	0·04	0·09	0·06	0·06
$(Ce/Ce^*)_N$[2]	11·80	1·25	2·90	1·08	0·77	13·03	1·14	0·95	1·15	0·99	1·58	30·81	1·18	1·09	1·06	1·22	1·90	1·66	1·34	5·35	4·02	2·99	6·85
Th/U	1·8	1·3	0·8	0·9	0·8	1·7	0·7	2·0	1·2	1·7	0·8	2·7	1·1	1·8	0·8	2·4	2·0	0·7	1·3	1·3	0·6	0·8	1·3
Nb/Ta	1·1	1·7	0·7	1·5	1·2	1·9	1·4	1·1	1·1	1·7	1·4	1·1	1·8	2·3	1·3	1·3	1·2	1·0	1·6	1·8	1·3	1·5	2·0
Yb/Sm	66·6	43·6	39·5	14·4	14·3	49·3	14·6	45·0	30·0	37·1	25·1	63·3	6·4	5·9	6·6	14·7	55·0	38·4	8·3	39·8	46·6	36·3	55·3
$(\Sigma REE + Y):P$[3]	10·8	12·1	9·8	13·9	13·1	11·2	7·9	10·6	11·8	12·2	8·5	7·7	14·6	15·9	11·7	8·1	10·5	5·2	8·3	7·3	3·6	7·5	7·1

Abundances are given in ppm. Av., average of two integrations.
[1]Normalized to chondritic values of McDonough & Sun (1995), calculated as $[Eu_N/(Sm_N + Gd_N)2]$.
[2]Normalized to chondritic values of McDonough & Sun (1995), calculated as $[Ce_N/(La_N + Pr_N)/2]$.
[3]Ratio calculated for cationic REE, Y, and P.

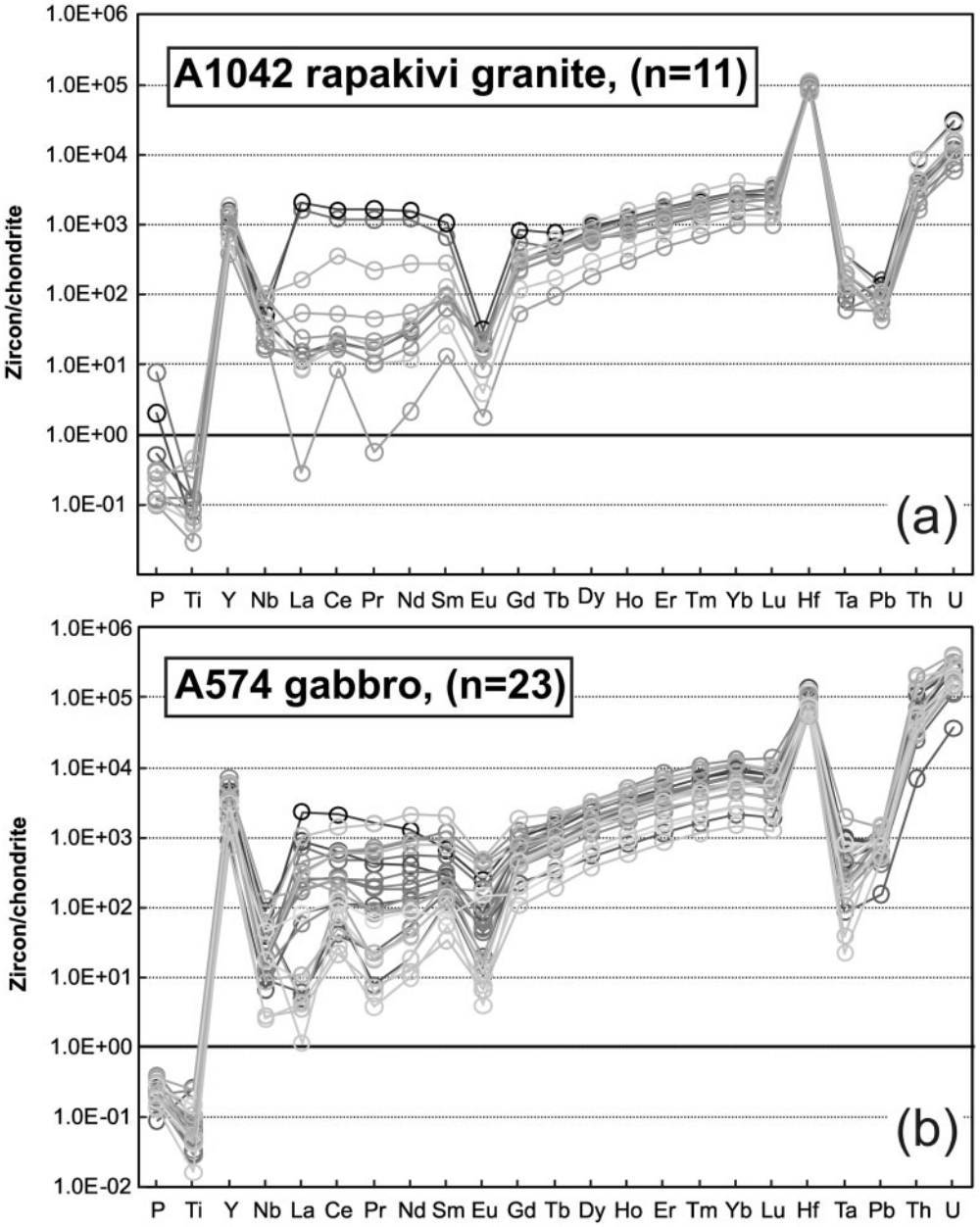

Fig. 6. Chondrite-normalized (McDonough & Sun, 1995) trace element abundances of zircons from samples (a) Al042 and (b) A574.

form of charge-balancing mechanism is needed to substitute all the trivalent cations in these zircons.

DISCUSSION

Boundary conditions for petrogenetic modelling

Rapakivi suites are an important subgroup of AMCG associations. The only consensus that the recent discussion surrounding the applicable classification (e.g. Frost *et al.*, 2001; Dall'Agnol & de Oliveira, 2007) and tectonic environment (Ashwal, 2008; Corrigan, 2008; McLelland *et al.*, 2008) of the rocks in these magmatic suites has produced is of petrogenetic ambiguity. It is very likely that a generalized petrogenetic model covering all of them does not exist. Therefore it is important to recognize the key petrogenetic features that distinguish granitic rocks previously pooled into the A-type clan from each other and search for common denominators that could be used in their further regrouping and reclassification.

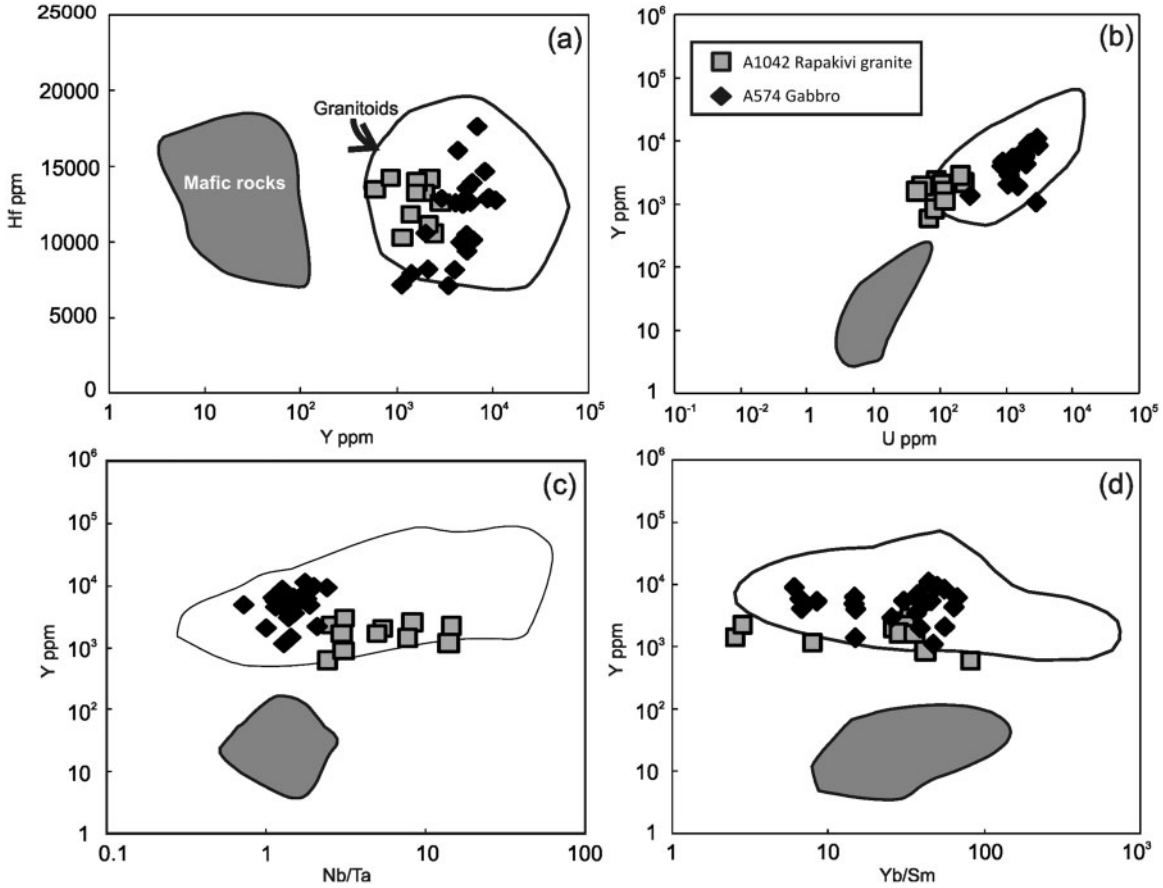

Fig. 7. Trace element discrimination diagrams of zircons from samples A1042 and A574. Mafic rock and granitoid fields according to data from Belousova *et al.* (2002).

In general, a mantle component is considered critical in petrogenetic models proposed for ferroan (A-type) granites and massif-type anorthosites (e.g. Haapala & Rämö, 1990; Emslie *et al.*, 1994; Mitchell *et al.*, 1995; Frost & Frost, 1997; Frost *et al.*, 2002). Whether this is a MORB-source depleted mantle component or a less depleted (or enriched) sub-continental lithosphere mantle component (Andersen *et al.*, 2009) is not known for certain.

Rämö (1991) discussed the genesis of the Finnish rapakivi granites and associated rocks in the light of elemental and Nd and Pb isotope geochemistry, and favored a model involving, at the outset, a basaltic partial melt from the upper mantle (probably produced by decompression melting and underplating associated with extension). This mafic melt was emplaced at the base of the crust at *c.* 1650 Ma and caused partial melting of the Svecofennian (1930–1830 Ma) lower crust, leading to the generation of silicic magmas from which the rapakivi granite batholiths were crystallized. The anorthositic and monzodioritic rocks were considered differentiates of the primary basaltic magma, contaminated to varying degrees by crustal material. These mafic differentiates were subsequently emplaced alongside the silicic magmas to form the (more evolved) mafic and intermediate counterparts of the rapakivi association (Heinonen *et al.*, 2010). An extensive mafic underplate is also implied by the results of deep seismic studies of the southern Finland crust (Elo & Korja, 1993; Luosto *et al.*, 1990).

Structural and geochemical features of composite dikes (Rämö, 1991), and net veined structures in monzodiorites and granites (Alviola *et al.*, 1999) and other hybrid rocks (Salonsaari, 1995; Kosunen, 2004), indicate that mixing and mingling of coexisting silicic and mafic magmas are significant processes in the genesis of these rocks. In such magmatic systems, distinction of isotopic source signals is rendered even more difficult, and assessment of mantle and crust components, their intermixing relations and extent of contamination by different crustal materials pose a considerable challenge. *In situ* study of Hf isotopes in zircon has proved to be a useful tool in shedding new light on some of these problems (see Kemp *et al.*, 2007). First, the *in situ* technique is able to detect isotopic differences

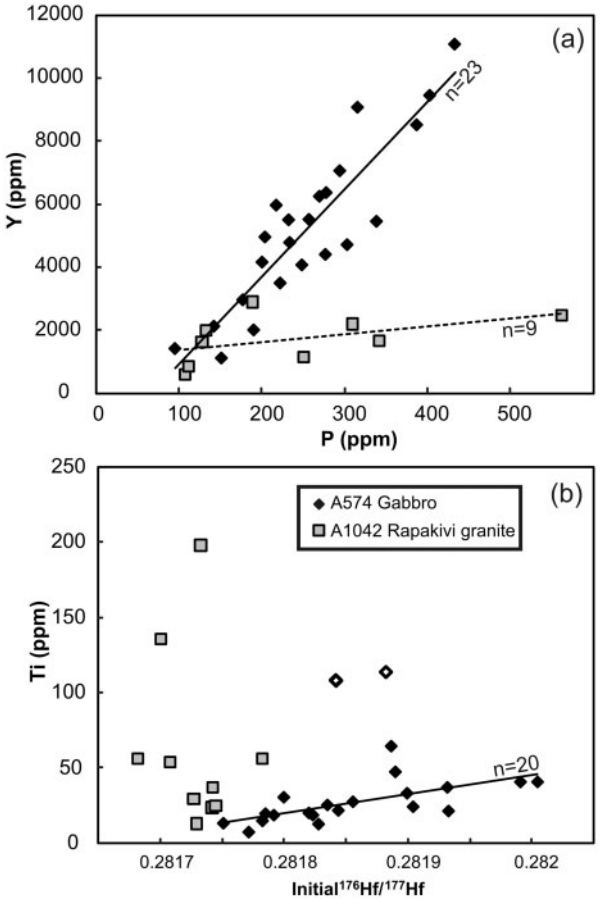

Fig. 8. (a) Plot of P (ppm) and Y (ppm) contents of zircon from samples A574 and Al042. Two analyses of zircon from sample Al042 with very high P were omitted for clarity of the plot. (b) Initial Hf isotope composition plotted against Ti content (ppm) of zircon from gabbro (A574) and rapakivi granite (Al042). Open diamonds refer to analyses from the gabbro omitted from the shown regression.

(if any) between single zircon grains, not just producing average values for macroscopic samples. Second, being more robust to post-magmatic alteration and mechanical effects than the whole-rock methods, zircon isotope studies can provide a firmer handle on the initial isotope composition of a magmatic system. Third, because Lu–Hf has a shorter half-life than Sm–Nd, Hf isotopes are more sensitive (producing more varying Hf isotope compositions, which in this study range from −2 to +9 ε_{Hf} units) than Nd isotopes in recording crustal (Svecofennian) components that formed only 300 Myr before the emplacement of the rapakivi granites.

Hf isotope composition of possible source reservoirs

To evaluate the contribution of different source materials in any given magmatic rock it is necessary to have reasonable estimates of the geochemical characteristics of the sources. The Hf isotope composition of the depleted mantle reservoir is here taken from Griffin *et al.* (2000), modified in agreement with the CHUR parameters of Bouvier *et al.* (2008). The crustal end-member evolution can be estimated from published Hf isotope data on granites in the Transscandinavian Igneous Belt and the Svecofennian Domain (Patchett *et al.*, 1981; Vervoort & Patchett, 1996; Andersen *et al.*, 2009; Kurhila *et al.*, 2010) and the two synorogenic post-kinematic granites (A588 and A924) analyzed in this study. Granites from the Svecofennian Domain in Finland indicate slightly less radiogenic Hf isotope compositions than granites of corresponding age in Sweden (ε_{Hf} at 1640 Ma ~−4 to +2 compared with ~−2 to +4, respectively), and probably represent the least radiogenic values of the Svecofennian crust at 1650–1550 Ma in southern Finland.

Hf isotope compositions of the rapakivi granites

The observed within-sample variation of Hf isotope compositions in the zircons from the rapakivi granite samples is comparable with the reproducibility on isotopically homogeneous reference zircons (±2 ε units), and significantly less than the up to 10 ε_{Hf} units that have been observed in samples of late Mesoproterozoic granites and early Mesoproterozoic tonalites and granodiorites of southwestern Fennoscandia (Andersen *et al.*, 2002, 2004, 2007). The two Svecofennian synorogenic post-kinematic granites (A588 and A924) also show insignificant within-sample variation of initial $^{176}Hf/^{177}Hf$. This homogeneity indicates that the zircon in each of the rapakivi granite samples crystallized from magma that was homogeneous in Hf isotopes.

The initial Hf compositions in the rapakivi granites are, with only one exception (A295), slightly higher than the estimated composition of the Svecofennian crust in southern Finland (A588 and A924; Kurhila *et al.*, 2010), but overlap with the inferred source of the granitic magmas of the Transscandinavian Igneous Belt (Fig. 5). This implies either a minor contribution of a mantle component to a well-homogenized granitic magma, or a high long-term Lu/Hf in a lower crustal source in the region, which would then resemble the lower crustal source of the Paleoproterozoic granitoids further west in Fennoscandia. Overall, the Hf isotope compositions of the rapakivi granites are consistent with the prevailing hypothesis that the Finnish rapakivi granites are mainly derived from a Svecofennian crustal source.

Nature of the mantle-derived component

The greater range in initial Hf isotope composition of zircons from the mafic rocks of the rapakivi association may yield a constraint not only for the source but also for the magmatic processes that led to the generation of these

rocks. Further evidence is available from comparing the initial Hf isotope composition with the trace-element composition of single zircon crystals from sample A574.

High actinide, Y, and HREE compositions of the zircons in gabbro sample A574 could suggest early precipitation of zircon from a mafic melt, but that control by crystal chemical effects efficiently hides information about further fractionation processes. The usefulness of REE in zircon as an indicator of fractionation has already been impugned by previous studies (e.g. Hoskin *et al.*, 2000) and is further questioned by the strong correlation of P and Y (representing general trivalent cations) in the zircons from this study (Fig. 8a). Despite continued efforts, no meaningful correlations between the Hf isotope and Th, U, Y, Pb, Nb, Ta, or REE variations in the zircons were found that could yield significant information about the differentiation of the parental melts. Of the analysed trace elements, tetravalent Ti, whose affinity for zircon is mainly controlled by temperature (Watson & Harrison, 2005), is probably the most reliable fractionation indicator. The range in Ti values within the observed fractionation window is from 40 to 10 ppm. This translates to a maximum temperature difference of *c.* 150°C (from ~900 to ~750°C; Ti-in-zircon thermometer of Ferry & Watson (2007); with ilmenite [$\log$ (Ti-in-zircon, ppm) $= 5{\cdot}711 \pm 0{\cdot}072 - 4800 \pm 86/T(\mathrm{K}) - \log a\mathrm{SiO_2} + \log a\mathrm{TiO_2}$ ($a\mathrm{TiO_2} = 1$ and $a\mathrm{SiO_2} = 1$)]), which (apart from the absolute temperature values) is a reasonable crystallization interval for a mafic melt at low-P (crustal) conditions. The Ti values and initial Hf isotope compositions of zircon in the gabbro (A574) correlate positively, implying gradually increasing incorporation of unradiogenic (crustal) Hf in the crystallizing zircons (Fig. 8b) during magmatic differentiation.

This effect could be caused by contamination of a mantle-derived primitive magma in which local zircon saturation is achieved at multiple levels during crystallization. As differentiation of the magma proceeded and the system cooled, the affinity of Ti for zircon fell in unison with the shift in isotope composition to crustal values by assimilation of crustal material. The highly radiogenic initial Hf isotope values (ε_{Hf} up to +9) recorded in some of the zircons in the mafic samples might therefore represent compositions close to the primary mantle source of the mafic rocks. This would imply that the previously reported whole-rock Nd isotope compositions of the basic rocks, ranging from ε values of −1·7 to +0·5 (Table 1 and references therein), do not record the original mantle signature, which would, according to the model above, be overprinted by the composition of the crustal contaminant. Thus the mantle source component involved in the generation of the classic rapakivi granites may have been closer to a MORB-source depleted mantle than a 'mildly depleted' lithospheric mantle (see Andersen *et al.*, 2009, and references therein).

Comparison with Nd and O isotopes

Given the insensitivity of the bulk-methods and the sparse geographical coverage of the samples it is not plausible to construct a detailed model for the crystallization processes involved. A rough consideration of the source components is, however, possible. We present a simple mixing model (Fig. 9) based on initial Hf isotope values, whole-rock Nd isotopes, and O isotope compositions in zircon (see Table 1). This model is compatible with the conditions for crustal and depleted mantle sources deduced in this study. The measured Nd isotope values are much more tightly spaced than the corresponding Hf isotope values; this reflects the relative resolution power of these two isotope systems.

Taking into consideration the uncertainties in the isotope composition of the more dominant crustal component, it is evident that the amount of possible mantle contribution to the granitic magmas is very difficult to constrain. The most extreme proportion of mantle material incorporated in the granites proposed by the model is almost 60%. In general, however, comparison between the three isotope systems provides valuable evidence for the homogeneity of the Hf isotope composition of the Svecofennian crust in southern Finland. The observation of Elliott *et al.* (2005) about the geographical control of stable oxygen isotope compositions in the rocks of the rapakivi association can also be seen in Fig. 9b. The southernmost silicic samples A1577 and A602 (Fig. 1) plot at significantly lower $\delta^{18}O$ values than the granites from farther north, suggesting that they have a source with less supracrustal contribution. The Hf isotope system holds no evidence for such variation—implying that the Svecofennian crust in Finland is homogeneous in terms of its overall Hf isotope composition.

Re-evaluation of rapakivi petrogenesis

The basic rocks of the Finnish rapakivi association record mildly depleted average initial Hf isotope compositions (Table 4) similar to selected central Fennoscandian Meso- to Neoproterozoic dolerites reported by Söderlund *et al.* (2005), which would suggest them to have a straightforward sub-continental lithospheric mantle (SCLM) source. Nevertheless, the *in situ* Hf analyses of their zircons (Figs 4 and 5) reveal a depleted mantle signal that is not present, for example, in their bulk Nd isotope compositions (e.g. Rämö, 1991).

The homogeneous initial Hf composition of the granitic samples also calls for an isotopically homogeneous source region. The SCLM of Fennoscandia is not plausible as a source as it is evidently characterized by a clearly, though mildly and variably depleted Hf isotope composition (Söderlund *et al.*, 2005). The homogeneity of the samples also precludes major contamination by more enriched (e.g. Archean crustal) material. Furthermore, Nd isotopes record the Archean crustal component in the rapakivi

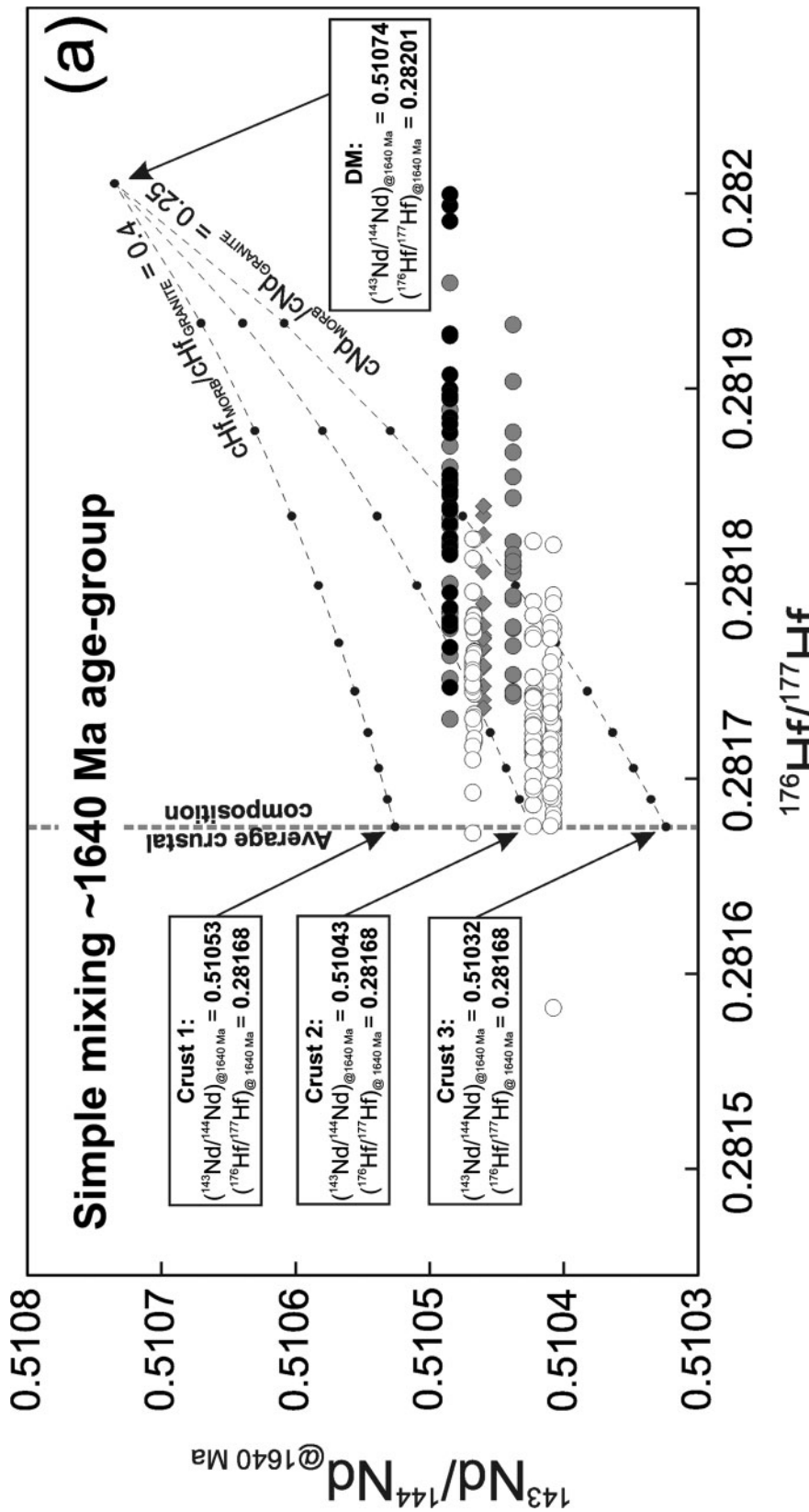

Fig. 9. Comparison of the single-zircon Hf isotope compositions with (a) whole-rock Nd and (b) zircon O isotope compositions showing possible magmatic end-members and crustal assimilates in a simple mixing scenario. DM, mantle Hf isotope composition is calculated to $t = 1640$ Ma, according to Griffin *et al.* (2000), with $\lambda = 1{\cdot}867 \times 10^{-11}\,a^{-1}$. Nd isotope composition is according to the DM model of DePaolo (1981). $\delta^{18}O$ mantle value according to Valley *et al.* (1998). Crust 1–3, Hf isotope composition is averaged from post-kinematic granites A588 and A924. Nd isotope compositions are modeled according to the initial isotope compositions obtained by Huhma (1986) and an averaged $^{147}Sm/^{144}Nd$ of 0·108 from the same samples. Crust2'; Hf isotope composition and $\delta^{18}O$ are averaged from post-kinematic granites A588 and A924. Crust3'; Hf isotope composition is averaged from post-kinematic granites A588 and A924. $\delta^{18}O$ value is the maximum value obtained by Hoefs & Epstein (1969) for Svecofennian crust in southern Finland. Concentration ratios in the approximated partial melts are estimated to be $cHf_{MORB}/cHf_{GRANITE}$ ~0·4 (0·2) and $cNd_{MORB}/cNd_{GRANITE}$ ~0·25 (Condie, 1993; Gao *et al.*, 1998; Farmer, 2004; Kelemen *et al.*, 2004; Kemp & Hawkesworth, 2004; Klein, 2004). Uncertainty (2SD) in Nd is ± 0·4 ε units and in $\delta^{18}O$ values ±0·1‰. Variation of the Hf isotope compositions is given at the 2SD level. Chondritic isotope compositions for Nd and Hf are according to DePaolo & Wasserburg (1976) and Bouvier *et al.* (2008) respectively. Oxygen isotope values are given as per mil deviation from VSMOW.

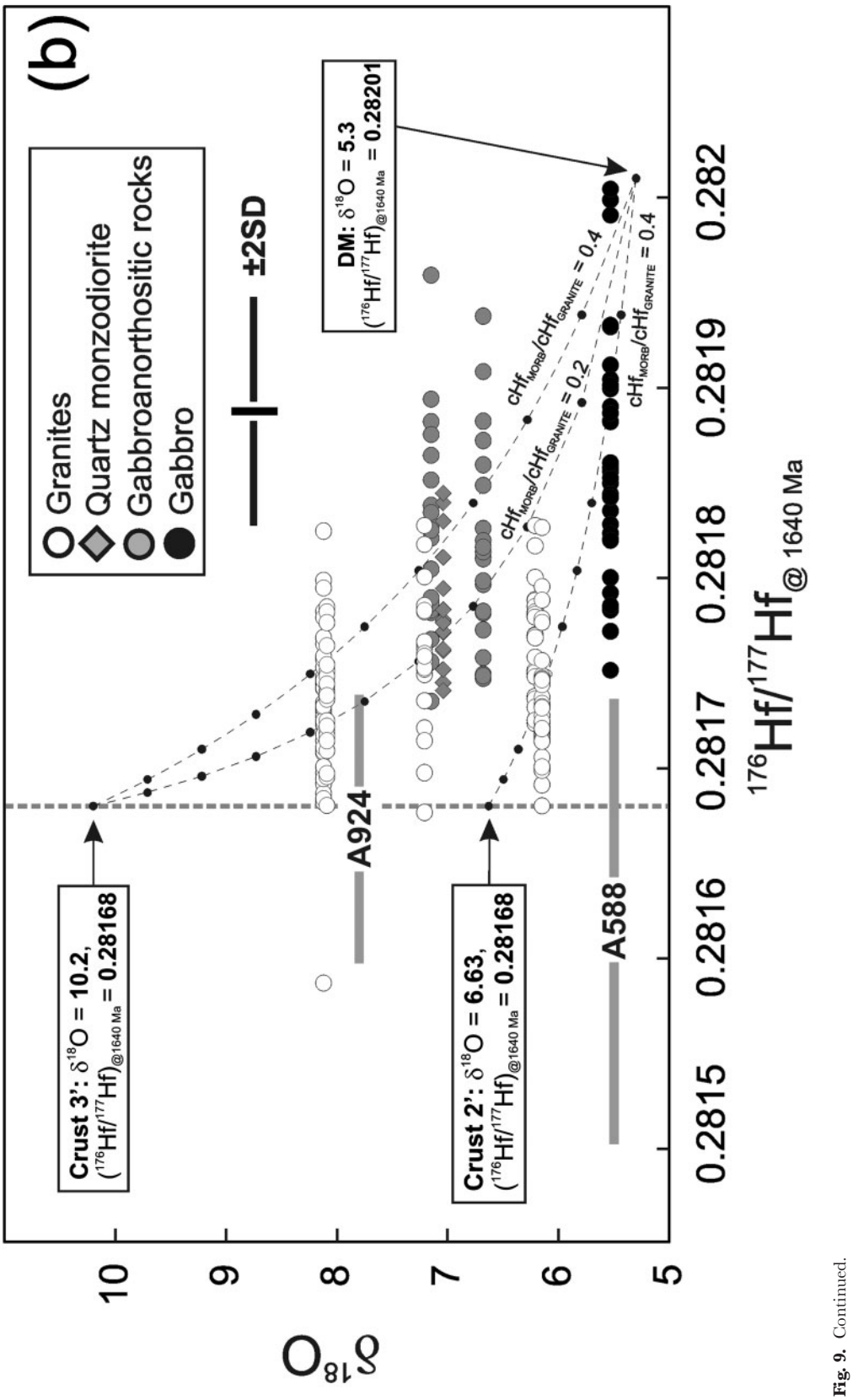

Fig. 9. Continued.

granites of the Salmi batholith, adjacent to the Archaean Karelian domain (e.g. Rämö, 1991; Neymark *et al.*, 1994), a signal that is absent from the Finnish rapakivi suite. Also, if the granites were straightforward mantle differentiates descended from the same lineage as the gabbro–anorthositic rocks (Turner *et al.*, 1992), a similar range in the variation of initial Hf isotope compositions should be evident in all the studied samples. The clearly more homogeneous Hf isotopes of the studied granites indeed point to the involvement of a rather homogeneous crustal source in their petrogenesis.

As a result of these observations, a truly bimodal petrogenetic model, with a MORB-source depleted mantle (or a highly depleted SCLM) source for the gabbro–anorthositic rocks and a major crustal source component for the rapakivi granites, is favored for the Finnish rapakivi association.

CONCLUSIONS

The Finnish rapakivi granites, formerly classified as A-type, are reduced (Dall'Agnol & de Oliveira, 2007) ferroan alkali–calcic (Frost *et al.*, 2001) granites that were emplaced in a well-characterized within-plate setting, not directly involved with coeval orogenesis. Judging by the Hf isotope record and trace-element compositions of the zircon in the granites and associated basic rocks observed in this study, it is inferred that two isotopically differing major sources are required for their petrogenesis.

We suggest that the primary source for the basic rocks associated with the rapakivi granites of southern Finland was a MORB-source depleted mantle; these mafic magmas were then affected by considerable crustal and/or SCLM contamination. The rapakivi granites have less radiogenic and more homogeneous initial Hf isotope compositions and we infer them to be the result of partial melting of Svecofennian crustal sources with a possible (minor) contribution from mantle-derived melts. The Svecofennian crust in southern Finland has a relatively homogeneous—almost chondritic—Hf isotope composition.

ACKNOWLEDGEMENTS

The assistance of Paula Kosunen, Helena Korkka, Siri Lene Simonsen and Juhani Virkanen in the field and in the laboratory is acknowledged. The Research Laboratory of the Finnish Geological Institute is thanked for kindly providing the sample material. Insightful comments from journal reviewers (Jon Patchett, Bernard Bonin and Tony Kemp) and the journal editor (Ron Frost) clearly improved our message. This paper is contribution no. 13 from the Department of Geosciences, University of Oslo Isotope Geology Laboratory, and publication number 81 of IGCP-510 (A-type Granites and Related Rocks through Time).

FUNDING

This work was supported by the University of Oslo grants, Småforsk program 2007–2009 (to T.A.) and the Academy of Finland (1215351 to O.T.R.).

SUPPLEMENTARY DATA

Supplementary data for this paper are available at *Journal of Petrology* online.

REFERENCES

Alviola, R. (1981). *Selostus Mäntyharjun Lovasjärven intruusiota koskevista teollisuusmineraalitutkimuksista vv. 1976–1978.* Geological Survey of Finland, Espoo (in Finnish).

Alviola, R., Johanson, B. S., Rämö, O. T. & Vaasjoki, M. (1999). The Proterozoic Ahvenisto rapakivi-massif-type anorthosite complex, southeastern Finland; petrography and U–Pb chronology. *Precambrian Research* **95**, 89–107.

Andersen, T., Griffin, W. L. & Pearson, N. J. (2002). Crustal evolution in the SW part of the Baltic Shield: the Hf isotope evidence. *Journal of Petrology* **43**, 1725–1747.

Andersen, T., Griffin, W. L., Jackson, S. E., Knudsen, T.-L. & Pearson, N. J. (2004). Mid-Proterozoic magmatic arc evolution at the southwest margin of the Baltic Shield. *Lithos* **73**, 289–318.

Andersen, T., Griffin, W. L. & Sylvester, A. G. (2007). Sveconorwegian underplating in southwestern Fennoscandia: LAM-ICPMS Hf isotope evidence from granites and gneisses in Telemark, southern Norway. *Lithos* **93**, 273–287.

Andersen, T., Andersson, U. B., Graham, S., Åberg, G. & Simonsen, S. L. (2009). Granitic magmatism by melting of juvenile continental crust: New constraints on the source of Paleoproterozoic granitoids in Fennoscandia from Hf isotopes in zircon. *Journal of the Geological Society, London* **166**, 233–247.

Anderson, J. L. (1983). Proterozoic anorogenic granite plutonism of North America. In: Medaris, L. G., Jr, Byers, C. W., Mickelson, D. M. & Shanks, W. C. (eds) *Proterozoic Geology, Selected Papers from an International Proterozoic Symposium. Geological Society of America, Memoirs* **161**, 133–154.

Andersson, U. B. (1997). Petrogenesis of some Proterozoic granitoid suites and associated basic rocks in Sweden (geochemistry and isotope geology). *Sveriges Geologiska Undersökning, Rapporter och Meddelanden Nr* **91**, 1–216.

Ashwal, L. D. (1993). *Anorthosites.* Berlin: Springer.

Ashwal, L. D. (2008). Proterozoic magmatism: How can we constrain tectonic setting? *Quebec 2008, GAC–MAC Meeting Abstracts* **33**, 8.

Belousova, E. A., Walters, S., Griffin, W. L., O'Reilly, S. Y. & Fisher, N. I. (2002). Zircon trace-element compositions as indicators of source rock type. *Contributions to Mineralogy and Petrology* **143**, 602–622.

Bergman, L. (1986). Structure and mechanism of intrusion of postorogenic granites in the archipelago of southwestern Finland. *Acta Academica Aboensis, Seria B, Mathematica et Physica, Matematik Naturvetenskaper, Teknik* **46**, 74.

Bonin, B. (2007). A-type granites and related rocks: Evolution of a concept, problems and prospects. *Lithos* **97**, 1–29.

Bouvier, A., Vervoort, J. & Patchett, P. J. (2008). The Lu–Hf and Sm–Nd isotopic composition of CHUR: Constraints from unequilibrated chondrites and implications for the bulk composition of terrstrial planets. *Earth and Planetary Science Letters* **273**, 48–57.

Chu, N. C., Taylor, R. N., Chavagnac, V., Nesbitt, R. W., Boella, R. M., Milton, J. A., German, C. R., Bayon, G. & Burton, K. (2002). Hf isotope ratio analysis using multi-collector inductively coupled plasma mass spectrometry: an evaluation of isobaric interference corrections. *Journal of Analytical Atomic Spectrometry* **17**, 1567–1574.

Condie, K. C. (1993). Chemical composition and evolution of the upper continental crust: contrasting results from surface samples and shales. *Chemical Geology* **104**, 1–37.

Corrigan, D. (2008). Tectonic setting of Proterozoic anorthosite massifs. *Quebec 2008 GAC–MAC Meeting Abstracts* **33**, 36.

Dall'Agnol, R. & de Oliveira, D. C. (2007). Oxidized, magnetite-series, rapakivi-type granites of Carajás, Brazil: Implications for classification and petrogenesis of A-type granites. *Lithos* **93**, 215–233.

DeBievre, P. & Taylor, P. D. P. (1993). Table of the isotopic composition of the elements. *International Journal of Mass Spectrometry and Ion Processes* **123**, 149–166.

DePaolo, D. J. (1981). Neodymium isotopes in the Colorado Front Range and crust–mantle evolution in the Proterozoic. *Nature* **291**, 193–196.

DePaolo, D. J. & Wasserburg, G. J. (1976). Nd isotopic variations and petrogenetic models. *Geophysical Research Letters* **3**, 249–252.

Duchesne, J.-C. & Wilmart, E. (1997). Igneous charnockites and related rocks from the Bjerkreim–Sokndal layered intrusion (southwest Norway): a jotunite (hyperstene monzodiorite)-derived A-type granitoid suite. *Journal of Petrology* **38**, 337–369.

Elliott, B. A. (2003). Petrogenesis of post-kinematic magmatism of the Central Finland Granitoid Complex II; sources and magmatic evolution. *Journal of Petrology* **44**, 1681–1701.

Elliott, B. A., Peck, W. H., Rämö, O. T., Vaasjoki, M. & Nironen, M. (2005). Magmatic zircon oxygen isotopes of 1·88–1·87 Ga orogenic and 1·65–1·54 Ga anorogenic magmatism in Finland. *Mineralogy and Petrology* **85**, 223–241.

Elo, S. & Korja, A. (1993). Geophysical interpretation of the crustal and upper mantle structure in the Wiborg rapakivi area, southeastern Finland. *Precambrian Research* **64**, 273–288.

Emslie, R. F. (1978). Anorthosite massifs, rapakivi granites, and late Proterozoic rifting in North America. *Precambrian Research* **7**, 61–98.

Emslie, R. F., Hamilton, M. A. & Thériault, R. J. (1994). Petrogenesis of a Mid-Proterozoic anorthosite–mangerite–charnockite–granite (AMCG) complex: isotope and chemical evidence from the Nain Plutonic suite. *Journal of Geology* **102**, 539–558.

Farmer, G. L. (2004). *Continental Basaltic Rocks*. In: Holland, H. D. & Turekian, K. K. (eds) *Treatise on Geochemistry, 3.* Amsterdam: Elsevier, pp. 85–121.

Ferry, J. M. & Watson, E. B. (2007). New thermodynamic models and revised calibrations for the Ti-in-zircon and Zr-in-rutile thermometers. *Contributions to Mineralogy and Petrology* **154**, 429–437.

Frost, B. R., Barnes, C. G., Collins, W. J., Arculus, R. J., Ellis, D. J. & Frost, C. D. (2001). A geochemical classification for granitic rocks. *Journal of Petrology* **42**, 2033–2048.

Frost, C. D. & Frost, B. R. (1997). Reduced rapakivi-type granites: The tholeiite connection. *Geology* **25**, 647–650.

Frost, C. D., Frost, B. R., Chamberlain, K. R. & Edwards, B. R. (1999). Petrogenesis of the 1·43 Ga Sherman batholith, SE Wyoming, USA: a reduced rapakivi-type anorogenic granite. *Journal of Petrology* **40**, 1771–1802.

Frost, C. D., Frost, B. R., Bell, J. M. & Chamberlain, K. R. (2002). The relationship between A-type granites and residual magmas from anorthosite: evidence from the northern Sherman batholith, Laramie Mountains, Wyoming, USA. *Precambrian Research* **119**, 45–71.

Frost, C. D., Rämö, O. T. & Dall'Agnol, R. (2007). IGCP project 510—A type granites and related rocks through time. *Lithos* **97**, vii–xiii.

Gao, S., Luo, T.-C., Zhang, B.-R., Zhang, H.-F., Han, Y.-W., Zhao, Z.-D. & Hu, Y.-K. (1998). Chemical composition of the continental crust as revealed by studies in East China. *Geochimica et Cosmochimica Acta* **62**, 1959–1975.

Griffin, W. L., Pearson, N. J., Belousova, E., Jackson, S. E., van Achterbergh, E., O'Reilly, S. Y. & Shee, S. R. (2000). The Hf isotope composition of cratonic mantle: LAM-MC-ICPMS analysis of zircon megacrysts in kimberlites. *Geochimica et Cosmochimica Acta* **64(1)**, 133–147.

Haapala, I. (1977). *Petrography and geochemistry of the Eurajoki stock, a rapakivi granite complex with greisen-type mineralization in southwestern Finland. Geological Survey of Finland, Bulletin* **286**, , 128 p.

Haapala, I. & Rämö, O. T. (1990). Petrogenesis of rapakivi granites of Finland. In: Stein, H. J. & Hannah, J. L. (eds) *Ore-bearing Granite Systems: Petrogenesis and Mineralizing Processes. Geological Society of America, Special Papers* **246**, 275–286.

Haapala, I. & Rämö, O. T. (1992). Tectonic setting and origin of the Proterozoic rapakivi granites of southeastern Fennoscandia. *Transactions of the Royal Society of Edinburgh, Earth Sciences* **83**, 165–171.

Heinonen, A. P., Rämö, O. T., Mänttäri, I., Johanson, B. & Alviola, R. (2010). Formation and fractionation of high-Al tholeiitic magmas in the Ahvenisto rapakivi granite-massif-type anorthosite complex, southeastern Finland. *Canadian Mineralogist* (in press).

Hoefs, J. & Epstein, J. (1969). O^{18}/O^{16} ratios of minerals from migmatites, rapakivi granites and orbicular rocks. *Lithos* **2**, 1–8.

Högdahl, K., Andersson, U. B. & Eklund, O. (eds) (2004). *The Transscandinavian Igneous Belt (TIB) in Sweden; a Review of its Character and Evolution. Geological Survey of Finland, Special Paper* **37**.

Hoskin, P. W. O. (2005). Trace-element composition of hydrothermal zircon and the alteration of Hadean zircon from the Jack Hills, Australia. *Geochimica et Cosmochimica Acta* **69**, 637–648.

Hoskin, P. W. O. & Schaltegger, U. (2003). The composition of zircon and igneous and metamorphic petrogenesis. In: Hanchar, J. M. & Hoskin, P. W. O. (eds) *Zircon. Mineralogical Society of America and Geochemical Society, Reviews in Mineralogy and Geochemistry* **53**, 27–62.

Hoskin, P. W. O., Kinny, P. D., Wyborn, D. & Chappell, B. W. (2000). Identifying accessory mineral saturation during differentiation in granitoid magmas: an integrated approach. *Journal of Petrology* **41**, 1365–1396.

Huhma, H. (1986). *Sm–Nd, U–Pb and Pb–Pb isotope evidence for the origin of the Early Proterozoic Svecokarelian crust in Finland. Geological Survey of Finland Bulletin* **337**, 48 p.

Kelemen, P. B., Hanghoj, K. & Greene, A. R. (2004). One view of the geochemistry of subduction-related magmatic arcs, with an emphasis on primitive andesite and lower crust. In: Holland, H. D. & Turekian, K. K. (eds) *Treatise on Geochemistry, 3.* Amsterdam: Elsevier, pp. 593–659.

Kemp, A. I. S. & Hawkesworth, C. J. (2004). Granitic perspectives on the generation and secular evolution of the continental crust. In: Holland, H. D. & Turekian, K. K. (eds) *Treatise on Geochemistry, 3.* Amsterdam: Elsevier, pp. 349–410.

Kemp, A. I. S., Hawkesworth, C. J., Foster, G. L., Paterson, B. A., Woodhead, J. D., Hergt, J. M., Gray, C. M. & Whitehouse, M. J. (2007). Magmatic and crustal differentiation history of granitic rocks from Hf–O isotopes in zircon. *Science* **315**, 980–983.

Klein, E. M. (2004). Geochemistry of the igneous oceanic crust. In: Holland, H. D. & Turekian, K. K. (eds) *Treatise on Geochemistry, 3*. Amsterdam: Elsevier, pp. 433–463.

Kosunen, P. (2004). Petrogenesis of mid-Proterozoic A-type granites: case studies from Fennoscandia (Finland) and Laurentia (New Mexico). PhD Thesis, University of Helsinki.

Kurhila, M., Andersen, T. & Rämö, O. T. (2010). Diverse sources of crustal granitic magma: Lu–Hf isotope data on zircon in three Paleoproterozoic leucogranites of southern Finland. *Lithos* **115**, 263–271.

Loiselle, M. C. & Wones, D. R. (1979). Characteristics of anorogenic granites. *Geological Society of America Abstracts with Programs* **11**, 468.

Longhi, J., Vander Auwera, J., Fram, M. S. & Duchesne, J. C. (1999). Some phase equilibrium constraints on the origin of Proterozoic (Massif) anorthosites and related rocks. *Journal of Petrology* **40**, 339–362.

Luosto, U., Tiira, T., Korhonen, H., Azbel, I., Burmin, V., Buyanov, A., Kosminskaya, I., Ionkis, V. & Sharov, N. (1990). Crust and upper mantle structure along the DSS Baltic profile in SE Finland. *Geophysical Journal International* **101**, 89–110.

McDonough, W. F. & Sun, S. S. (1995). The composition of the Earth. *Chemical Geology* **120**, 223–253.

McLelland, M., Bickford, M. E. & Hamilton, M. A. (2008). Zircon geochronology and the tectonic environment of anorthosites. *Quebec 2008 GAC–MAC Meeting Abstracts* **33**, 109.

Mitchell, J. N., Scoates, J. S. & Frost, C. D. (1995). High-Al gabbros in the Laramie Anorthosite Complex, Wyoming: implications for the composition of melts parental to Proterozoic anorthosite. *Contributions to Mineralogy and Petrology* **119**, 166–180.

Neymark, L. A., Amelin, Y. V. & Larin, A. M. (1994). Pb–Nd–Sr isotope and geochemical constraints on the origin of the 1·54–1·56 Ga Salmi rapakivi granite–anorthosite batholith (Karelia, Russia). *Mineralogy and Petrology* **50**, 173–193.

Patchett, P. J., Kouvo, O., Hedge, C. E. & Tatsumoto, M. (1981). Evolution of continental crust and mantle heterogeneity: evidence from Hf isotopes. *Contributions to Mineralogy and Petrology* **78**, 279–297.

Rämö, T. (1991). *Petrogenesis of Proterozoic rapakivi granites and related basic rocks of southeastern Fennoscandia: Nd and Pb isotopic and general geochemical constraints. Geological Survey of Finland, Bulletin* **355**.

Rämö, O. T. & Haapala, I. (2005). Rapakivi granites. In: Lehtinen, M., Nurmi, P. A. & Rämö, O. T. (eds) *Precambrian Geology of Finland—Key to the Evolution of the Fennoscandian Shield*. Amsterdam: Elsevier, pp. 533–562.

Rämö, O. T., Huhma, H. & Kirs, J. (1996). Radiogenic isotopes of the Estonian and Latvian rapakivi granite suites: new data from the concealed Precambrian of the East European Craton. *Precambrian Research* **79**, 209–226.

Rämö, O. T., Vaasjoki, M., Mänttäri, I., Elliott, B. A. & Nironen, M. (2001). Petrogenesis of the post-kinematic magmatism of the Central Finland Granitoid Complex I; radiogenic isotope constraints and implications for crustal evolution. *Journal of Petrology* **42**, 1971–1993.

Rämö, O. T., Mänttäri, I., Harju, S., Luttinen, A. V., Kohonen, J. & Heinonen, A. P. (2009). Volcanism associated with the Proterozoic Wiborg rapakivi granite batholith. *EOS Transactions, American Geophysical Union* **90(22)**, Joint Assembly Supplement, Abstract GA11A-02.

Salonsaari, P. (1995). Hybridization in the subvolcanic Jaala-Iitti complex and its petrogenetic relation to rapakivi granites and associated mafic rocks of Southeastern Finland. *Geological Society of Finland, Bulletin* **67** (part 1b).

Scherer, E., Münker, C. & Mezger, K. (2001). Calibration of the lutetium–hafnium clock. *Science* **293**, 683–687.

Scherer, E. E., Münker, C. & Mezger, K. (2007). The Lu–Hf systematics of meteorites: Consistent or not. *Goldschmidt Conference Abstracts 2007. Geochimica et Cosmochimica Acta* **71(15S)**, A888.

Schiellerup, H., Lambert, D. D., Prestvik, T., Robins, B., McBride, J. S. & Larsen, R. B. (2000). Re–Os isotopic evidence for a lower crustal origin of massif-type anorthosites. *Nature* **405**, 781–784.

Scoates, J. S. & Mitchell, J. N. (2000). The evolution of troctolitic and high-Al basaltic magmas in Proterozoic anorthosite plutonic suites and implications for the Voisey's Bay massive Ni–Cu sulfide deposit. *Economic Geology* **95**, 677–701.

Segal, I., Halicz, L. & Platzner, I. T. (2003). Accurate isotope ratio measurements of ytterbium by multiple collection inductively coupled plasma mass spectrometry applying erbium and hafnium in an improved double external normalization procedure. *Journal of Analytical Atomic Spectrometry* **18**, 1217–1223.

Siivola, J. (1987). Lovasjärven mafinen intruusio. *Geological Survey of Finland, Report of Investigation* **76**, 121–128 (in Finnish).

Söderlund, U., Patchett, P. J., Vervoort, J. D. & Isachsen, C. E. (2004). The ^{176}Lu decay constant determined by Lu–Hf and U–Pb isotope systematics of Precambrian mafic intrusions. *Earth and Planetary Science Letters* **219**, 311–324.

Söderlund, U., Isachsen, C. E., Bylund, G., Heaman, L. M., Patchett, P. J., Vervoort, J. D. & Andersson, U. B. (2005). U–Pb baddeleyite ages and Hf, Nd isotope chemistry constraining repeated mafic magmatism in the Fennoscandian Shield from 1.6 to 0.9 Ga. *Contributions to Mineralogy and Petrology* **150**, 174–194.

Suominen, V. (1991). *The chronostratigraphy of southwestern Finland with special reference to Postjotnian and Subjotnian diabases. Geological Survey of Finland, Bulletin* **356**, 100 p.

Turkki, V. (2005). Pyhtään Ristisaaren kallioperä ja sen tumma wiborgiitti, MSc thesis, University of Helsinki.

Turner, S. P., Foden, J. D. & Morrison, R. S. (1992). Derivation of some A-type magmas by fractionation of basaltic magma: An example from the Padthaway Ridge, South Australia. *Lithos* **28**, 151–179.

Vaasjoki, M. (1977). *Rapakivi granites and other postorogenic rocks in Finland: their age and the lead isotopic composition of certain associated mineralizations. Geological Survey of Finland, Bulletin* **294**, 64 p.

Vaasjoki, M., Rämö, O. T. & Sakko, M. (1991). New U–Pb ages from the Wiborg rapakivi area: constraints on the temporal evolution of the rapakivi granite–anorthosite–diabase dyke association of southeastern Finland. *Precambrian Research* **51**, 227–243.

Valley, J. W., Kinny, P. D., Schulze, D. J. & Spicuzza, M. J. (1998). Zircon megacrysts from kimberlite: Oxygen isotope heterogeneity among mantle melts. *Contributions to Mineralogy and Petrology* **133**, 1–11.

Vander Auwera, J., Longhi, J. & Duchesne, J. C. (1998). A liquid line of descent of jotunite (hypersthene monzodiorite) suite. *Journal of Petrology* **39**, 439–468.

Vervoort, J. D. & Patchett, P. J. (1996). Behaviour of hafnium and neodymium isotopes in the crust: Constraints from Precambrian crustally derived granites. *Geochimica et Cosmochimica Acta* **60(19)**, 3717–3733.

Vorma, A. (1976). *On the petrochemistry of rapakivi granites with special reference to the Laitila massif, southwestern Finland. Geological Survey of Finland Bulletin* **285**.

Watson, E. B. & Harrison, T. M. (2005). Zircon thermometer reveals minimum melting conditions on earliest Earth. *Science* **308**, 841–844.

Woodhead, J. D. & Hergt, J. M. (2005). A preliminary appraisal of seven natural zircon reference materials for *in situ* Hf isotope determination. *Geostandards and Geoanalythical Research* **29**, 183–195.